Cardiac proteomics reveals sex chromosome-dependent differences between males and females that arise prior to gonad formation

Wei Shi,[1,5] Xinlei Sheng,[2,5] Kerry M. Dorr,[1] Josiah E. Hutton,[2] James I. Emerson,[1] Haley A. Davies,[1] Tia D. Andrade,[1] Lauren K. Wasson,[1] Todd M. Greco,[2] Yutaka Hashimoto,[2] Joel D. Federspiel,[2] Zachary L. Robbe,[1] Xuqi Chen,[4] Arthur P. Arnold,[4] Ileana M. Cristea,[2,*] and Frank L. Conlon[1,3,6,*]

[1]Department of Biology and Genetics, McAllister Heart Institute, UNC-Chapel Hill, Chapel Hill, NC 27599, USA
[2]Department of Molecular Biology, Princeton University, Lewis Thomas Laboratory, Washington Road, Princeton, NJ 08544, USA
[3]Lineberger Comprehensive Cancer Center, University of North Carolina at Chapel Hill, Chapel Hill, NC 27599, USA
[4]Department of Integrative Biology & Physiology, University of California, Los Angeles, Los Angeles, CA 90095, USA
[5]These authors contributed equally
[6]Lead contact
*Correspondence: icristea@princeton.edu (I.M.C.), frank_conlon@med.unc.edu (F.L.C.)
https://doi.org/10.1016/j.devcel.2021.09.022

SUMMARY

Sex disparities in cardiac homeostasis and heart disease are well documented, with differences attributed to actions of sex hormones. However, studies have indicated sex chromosomes act outside of the gonads to function without mediation by gonadal hormones. Here, we performed transcriptional and proteomics profiling to define differences between male and female mouse hearts. We demonstrate, contrary to current dogma, cardiac sex disparities are controlled not only by sex hormones but also through a sex-chromosome mechanism. Using Turner syndrome (XO) and Klinefelter (XXY) models, we find the sex-chromosome pathway is established by X-linked gene dosage. We demonstrate cardiac sex disparities occur at the earliest stages of heart formation, a period before gonad formation. Using these datasets, we identify and define a role for alpha-1B-glycoprotein (A1BG), showing loss of A1BG leads to cardiac defects in females, but not males. These studies provide resources for studying sex-biased cardiac disease states.

INTRODUCTION

Human sexual dimorphism is associated with differences in the prevalence of a wide variety of disease states, including cancer, cardiovascular disease, dementia, chronic kidney disease, obesity, and autoimmune disease. In the heart, sex disparities exist in the anatomy and physiology of cardiac tissues as well as in the preponderance of specific types of heart disease (Chester et al., 2018; Chlebowski et al., 2017; Dent et al., 2011; Garcia et al., 2016; Haberer and Silversides, 2019; Mosca et al., 2007; Prabhavathi et al., 2014; Whayne and Mukherjee, 2015; Wu et al., 2020). For example, females have a higher rate of atrial septal defects, while males exhibit a higher rate of aortic arch abnormalities (Arnold et al., 2001; Giannakoulas et al., 2017; Maric-Bilkan et al., 2016). Dissimilarities are accentuated in patient outcomes, in which women almost uniformly fare far worse than men (Chester et al., 2018; Chlebowski et al., 2017; Dent et al., 2011; Garcia et al., 2016; Haberer and Silversides, 2019; Prabhavathi et al., 2014; Whayne and Mukherjee, 2015; Wu et al., 2020). According to a report published in 2011, a woman dies of cardiovascular disease in the United States every minute (Mosca et al., 2011b).

Clinical studies have implicated sex hormones as an influencing factor in differing patient outcomes (Chester et al., 2018; Chlebowski et al., 2017; Dent et al., 2011; Garcia et al., 2016; Haberer and Silversides, 2019; Mosca et al., 2007; Prabhavathi et al., 2014; Whayne and Mukherjee, 2015; Wu et al., 2020). However, current studies suggest that a sex-specific program controlled genetically through the X or Y chromosome may function outside of the gonads to control protein expression (Arnold, 2017, 2019b; Naqvi et al., 2019; San Roman and Page, 2019; Snell and Turner, 2018). Though hormones play a critical role in cardiac disease, mechanisms underlying sex differences in cardiac homeostasis and disease remain unexplained.

To define the mechanisms of cardiac sex differences, we initiated transcriptional profiling and a quantitative proteomic-based approach to identify transcripts, proteins, protein complexes, and protein pathways differentially expressed in male versus female heart tissue. We have leveraged the power of the collaborative cross (CC) as a surrogate for human diversity, identifying processes that are conserved and those that diverge between males and females across heterogeneous populations. To determine whether these sex disparities in cardiac-protein expression are due, in part, to sex chromosome mechanisms, we quantified
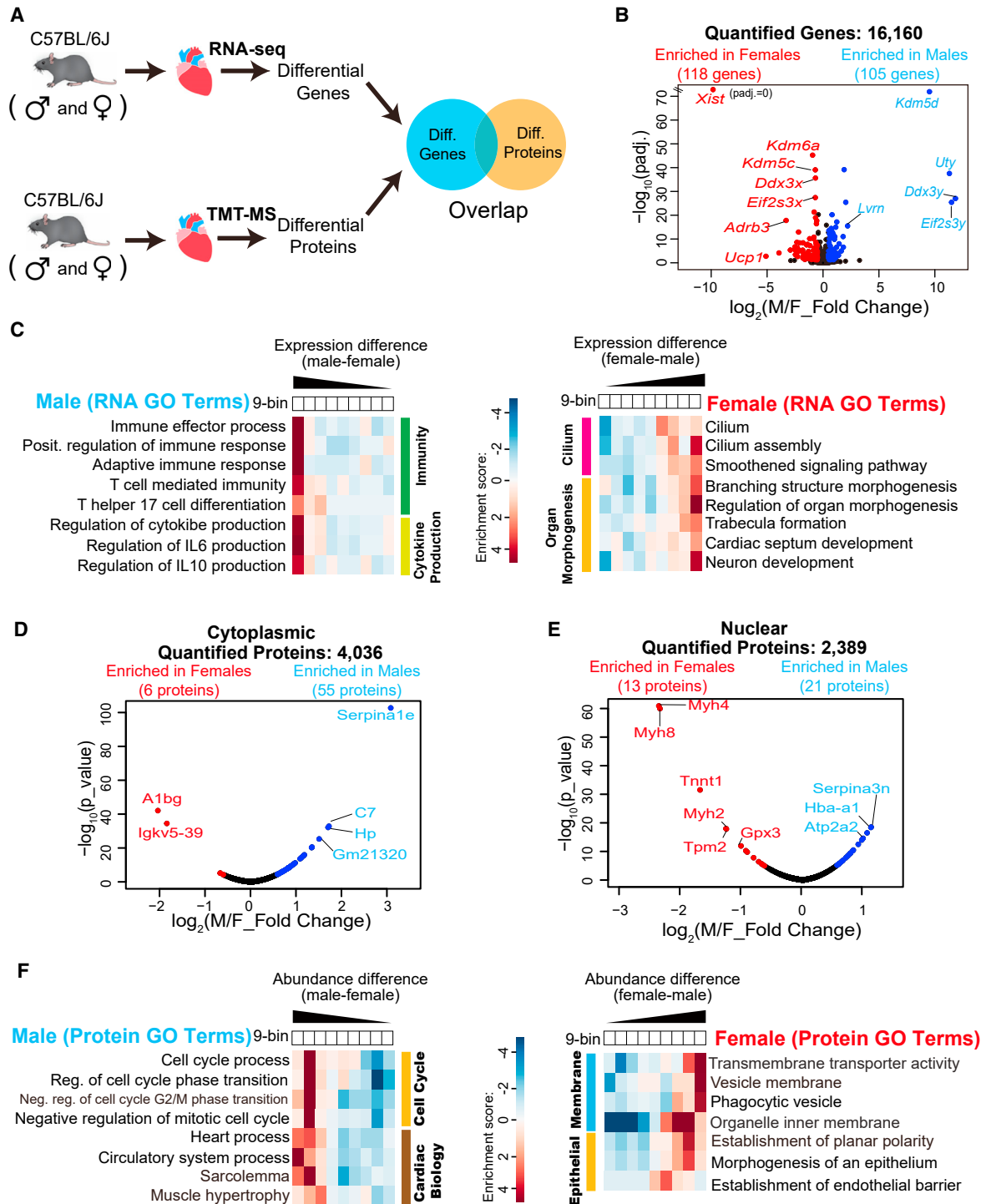
Figure 1. Cardiac transcriptome and proteome in C57BL/6J mouse

(A) Overview of the transcriptomics and proteomics analyses in C57BL/6J mouse hearts.

(B) Volcano plot of RNA-seq in C57 mouse hearts showing $\log_2$ (male/female fold change) plotted against $-\log_{10}$ padj. (adjusted p value) determined by DESeq2. Genes with $\log_2$ (male/female fold change) > 0.5 padj. < 0.05 enriched in male hearts, blue dots; $\log_2$ (male/female fold change) < −0.5 padj. < 0.05 enriched in female hearts, red dots. Representative genes in each sex labeled in the plot. n = 4 per sex.

(C) Representative enriched gene ontology (GO) terms (biological processes) of identified genes from C57 mouse hearts. Terms are divided into male-enriched (left) and female-enriched (right). Color bar: enrichment score.

protein levels in adult cardiac tissue derived from the four core genotypes (FCG) mouse model. In opposition to current studies, suggesting cardiac sex disparities are solely sex hormone driven (Arnold, 2017, 2019b; Snell and Turner, 2018), we demonstrate that a sex chromosome-complement mechanism contributes to cardiac sex disparities.

We have used our technologies and datasets to test the role of X-linked gene dosage in heart tissue, measuring cardiac-protein expression levels in Turners syndrome (XO) and Klinefelter (XXY) mouse models. These studies demonstrate the role of X-linked genes acting outside sex tissues to directly regulate cardiac-protein expression. As congenital heart disease (CHD) is frequently sex biased, we have used our approaches to determine if sex biases occur in the early mammalian heart. We find that mouse cardiomyocytes show sex-biased protein expression as early as E9.5, a period significantly earlier than gonadal expression of the testis-determining gene *Sry* and a period preceding mammalian gonadal development (Koopman et al., 1991) (Brennan and Capel, 2004). We went on to test the utility of these datasets for identifying proteins involved in cardiac disease by testing the role of the cardiac protein alpha-1B-glycoprotein (A1BG), a protein enriched in embryonic and adult female heart tissue. By generating a cardiac conditional allele of *A1bg*, we demonstrate that loss of *A1bg* leads to cardiac abnormalities in females but not males. Taken together, these findings demonstrate that sex-chromosome-complement pathways function to establish cardiac sex disparities prior to gonad formation.

RESULTS

Cardiac sex differences are established by post-transcriptional mechanisms

Males and females differ in the biology and physiology of their hearts. However, very few studies have investigated the quantitative differences of male-female heart tissue. To investigate the molecular basis of cardiac sex differences, we used an unbiased systems-based approach to characterize differential male and female cardiac transcripts in adult mouse hearts using RNA-sequencing (Figures 1A and 1B; Table S1A). From these studies, pathway analysis showed an enrichment in males (47%) in processes associated with the immune responses (Figure 1C, left), whereas females displayed enrichment (118/223) in cilium, septation, and trabeculation (Figure 1C, right). These results demonstrate that differences exist at the gene-expression level between male and female heart tissues.

RNA processing has an essential function in determining protein-expression levels (Jordan et al., 2019). To determine whether male-female cardiac RNA differences are related to disparities in protein abundances, we utilized quantitative mass spectrometry (MS) with tandem mass tags (TMT) (Figure 1A). To reduce sample complexity and to increase proteomic depth of coverage, we fractionated the heart tissue into cytoplasmic and nuclear fractions. Of the detected proteomes, only a subset of 95 cardiac proteins had differential abundances in male versus female (Figures 1D and 1E; Table S1B). Cardiac proteins that displayed sex differences were associated with biological processes that were disparate from those observed for differentially expressed mRNAs. Males showed enrichment in cell cycle and heart processes (Figure 1F, left), and females showed enrichment in membrane and epithelial-related pathways (Figure 1F, right).

Our results implied that sex disparities in cardiac-protein abundances occur, in part by post-transcriptional mechanisms. To test this hypothesis, we compared the levels of male and female proteins with our corresponding RNA-seq data. Only 4% (9/223) of the RNAs that displayed at least a 1.5-fold change between male and female exhibited corresponding changes at the protein level (Figures 1A and S1A–S1D). We conclude from these findings that a post-transcriptional mechanism contributes to male-female cardiac differences.

Conserved cardiac sex protein, protein complexes, and biological processes in heterogeneous populations

The CC (Churchill et al., 2004; Threadgill et al., 2011) is a panel of recombinant inbred mouse strains derived from eight founder strains that have, in aggregate, greater diversity than the total human population; thus, the CC is an appropriate surrogate for human genetic variation (Churchill et al., 2004; Saul et al., 2019; Threadgill and Churchill, 2012; Threadgill et al., 2011). To date, no RNA or protein analyses have been reported on heart tissue from the CC. Therefore, to identify the proteins and pathways for which cardiac sex differences are conserved across heterogeneous populations, we conducted TMT-MS analyses of male and female hearts across all eight CC founding mouse strains (Figures 2A, S1E–S1T, and S2; Tables S1C–S1E).

Bayesian modeling successfully identified a group of 1,379 differential male-female cardiac proteins across the founder strains (Figures 2B and S3B–S3G). Proteins were annotated into pathways associated with peptide synthesis and gene expression (cluster I), intracellular transport and protein localization (cluster II), protein localization to cell periphery (cluster III), and RNA processing (cluster IV) (Figure 2B; Table S1F). In general, the conserved cardiac pathways found to exhibit enhanced bias in males are involved in metabolic processes (Figure 2C, left), whereas the conserved pathways exhibiting female bias were associated with the architectures of the nucleus and the endoplasmic reticulum (Figure 2C, right). These groups of conserved, differentially regulated proteins include proteins previously reported to be associated with cardiac sex-biased disease states (Mosca et al., 2011a; Peters et al., 2019). For example, decreases in MAP4K4 protein levels have been associated with insulin-resistance, obesity, and atherosclerosis, all prevalent and often lethal female-biased disease states (Fiedler et al., 2020). Consistently, our results show higher MAP4K4 expression levels in male hearts (Figure 2B). Together, these findings identify a conserved set of proteins and pathways across founder strains,

(D and E) Volcano plots of TMT-MS in C57 mouse hearts in each cellular fraction: cytoplasmic (D) and nuclear (E) $\log_2$ (male/female fold change) plotted against the $-\log_{10}$ (p value). Proteins with $\log_2$ (male/female fold change) > 0.59, p value < 0.01 enriched in male hearts, blue dots; $\log_2$ (male/female fold change) < −0.59, p value < 0.01 enriched in female hearts, red dots. n = 2 per sex.

(F) Representative enriched GO terms (biological processes) of identified proteins from C57 mouse hearts. Color bar: enrichment score.

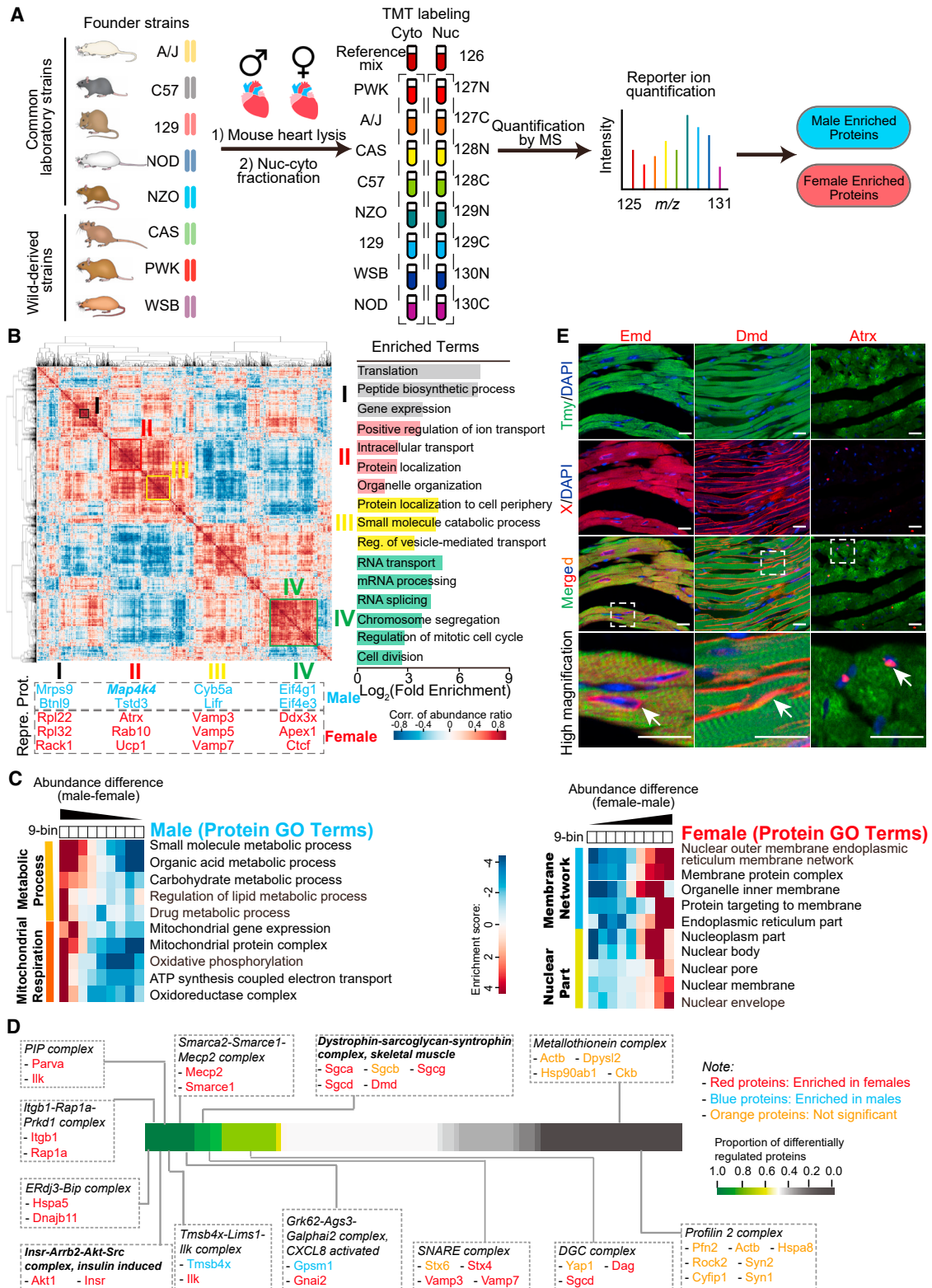See Figures S1, S2, S5C, and S5D and Tables S1A–S1D and S2.

Figure 2. Global cardiac proteome in the founder strains of the Collaborative Cross mice

(A) Design and TMT-MS proteomic workflow for hearts of eight founder CC strains. Abbreviations: C57, C57BL/6J; 129, 129S1/SvlmJ; NOD, NOD/ShiLtJ; NZO, NZO/H1LtJ; CAS, CAST/EiJ; PWK, PWK/PhJ; WSB, WSB/EiJ.

a subset of which appear to contribute to male-female disease bias.

Consistent with reported variabilities in gene expression between mouse strains (Fontaine and Davis, 2016; Hunter, 2012), our analyses further revealed diversity in sex-biased proteins and protein pathways by strain. For example, mouse strains PWK/PhJ and CAST/EiJ exhibit male bias in cardiac proteins expressed at the G2/M checkpoint, while NZO/HILtJ and NOD/ShiLtJ strains show female bias (Figure S3H). Additionally, strain 129S1/SvImJ shows male bias for oxidative phosphorylation, while all others demonstrate female bias (Figure S3I).

We further observed strain basis at the single protein level. MYH7 is the gene most frequently associated with cardiac hypertrophy (CH) (Homburger et al., 2016; Marian and Braunwald, 2017; Morita et al., 2008; Sabater-Molina et al., 2018). Women with CH have a significantly higher frequency of heart failure and death versus men (Olivotto et al., 2005; Regitz-Zagrosek and Seeland, 2011). Similarly, there are sex differences in response to hypertrophy modeling in mice (Böhm et al., 2013; Dieseldorff Jones et al., 2020; Harrington et al., 2017; Konhilas et al., 2015; Patrizio and Marano, 2016; Queirós et al., 2013; Shioura et al., 2008; Witt et al., 2008; Wu et al., 2003). We found MYH7 to be one of the most differentially regulated proteins between male and female and among the proteins that exhibited strain-dependent male-female regulation across all founder strains. Surprisingly, the two mouse strains that showed the greatest disparity are 129S1/SvImJ and C57BL/6J, two of the more common strains used in CH studies. 129S1/SvImJ showed a dramatic male increase in MYH7 and C57BL/6J showed a dramatic female increase (Figure S3J). Thus, these findings may help to explain some of the discrepancies in hypertrophic mouse models (Harrington et al., 2017). In total, data on the CC founding lines demonstrate significant differences between mouse strains in the cardiac proteins and pathways that demonstrate sex-biased expression.

Male-female differential protein complexes

Proteins assemble and function in multicomponent complexes. Consistent with female predisposition for upregulation in protein-expression levels for cytoplasmic proteins (772 versus 336) and nuclear proteins (218 versus 53) (Figures S3C and S3D; Table S1F), we found significant enrichments in protein complexes that are largely female biased. For example, we found female upregulation in proteins comprising the dystrophin complex (Figure 2D), which, when mutated, leads to sex differences in the pathways of muscle wasting (Arnold et al., 2001; Giannakoulas et al., 2017; Maric-Bilkan et al., 2016; Rosa-Cald-

well and Greene, 2019). A second example is the insulin-induced pathway protein complex that was also upregulated in females, and this pathway is known to be associated with female-biased obesity and cardiac disease (Arnold et al., 2001; Giannakoulas et al., 2017; ORIGIN Trial Investigators et al., 2012; Maric-Bilkan et al., 2016; Peters et al., 2019). In aggregate, our data utilizing founder strains have identified a core set and a set of strain-specific enriched cardiac proteins, protein complexes, and protein pathways from a heterogeneous population.

Cardiac sex disparities in cardiomyocytes

As our study analyzed whole-heart samples and the adult heart comprises multiple cell types, we sought to determine the cell types expressing the identified sex-based differential protein abundances. Western blot analyses of ATRX, DDX3X (DEAD-box helicase 3 X-linked), and PBDC1 (polysaccharide biosynthesis domain-containing protein 1) protein levels are upregulated in females (Figures S3F and S3G). We further found ATRX with EMD and DMD to be co-expressed with tropomyosin in the cardiomyocyte compartment of adult hearts (Figure 2E). Therefore, we conclude that cardiomyocytes can differentially express male and female proteins.

Cardiac sex disparities are established by gonadal hormonal and sex-chromosome mechanisms

Past studies have implied that sex differences in cardiac tissue are controlled by gonadal hormonal regulation (Blenck et al., 2016; Kararigas et al., 2014; Patrizio and Marano, 2016; Regitz-Zagrosek and Kararigas, 2017; Ventura-Clapier et al., 2017; Wu et al., 2020). However, other reports suggest that sex differences are also regulated by inequalities in sex chromosome complement (Arnold, 2017, 2019b; Snell and Turner, 2018). To determine whether sex disparities in cardiac-protein abundances are due, in part, to sex-chromosomal mechanisms, we quantified protein levels in adult cardiac tissue derived from the FCG mouse model (Arnold et al., 2017; Burgoyne and Arnold, 2016; Naqvi et al., 2019; Snell and Turner, 2018). The FCG model takes advantage of deletion of *Sry* (the Y chromosome testis-determining gene) and insertion of *Sry* into an autosome (Figure S3K). Testes develop in FCG mice, but gonadal sex is uncoupled from the sex chromosome complement (XX versus XY) (Burgoyne and Arnold, 2016; Snell and Turner, 2018).

Using the FCG model in three independent matings in the C57BL/6J background, we derived mice of all four genotypes and conducted TMT-MS analyses of the respective heart tissues (Figures 3A and S3K–S3M). Using this approach, we obtained quantitative measurements on 3,871 proteins in each of the

(B) Correlation matrix of sex differences across all eight founder strains. Protein abundance ratios (log$_2$ [male/female]) in eight strains were concatenated for each protein, and correlation of ratios was calculated between proteins. Color bar: correlation of abundance ratio (log$_2$ [male/female]). Four representative clusters are labeled in the heatmap (I–IV), representative enriched GO terms (FDR < 0.05, fold enrichment > 2; protein numbers involved in each term > 10) and representative proteins (repre. prot.) in each cluster, respectively, are shown.

(C) Representative enriched GO terms (biological processes) of identified proteins from the eight CC founder strains hearts of both sexes. Color bar: enrichment score.

(D) Differential protein complex analyses. Representative identified protein complexes from eight CC founder strains hearts are shown in dashed line squares. Proteins in red: enriched in females; in blue: enriched in males; in orange: not significant. Color bar: proportion of differentially regulated proteins.

(E) Representative immunohistochemistry (IHC) fluorescence staining in adult female C57 heart sections. Cardiomyocytes stained by tropomyosin (green), protein stained with Emd (emerin), Dmd (dystrophin), or Atrx (alpha thalassemia/mental retardation syndrome X-linked) antibody (red and white arrows), nucleus stained by DAPI (blue); scale bars: 25 μm. High magnification images showing areas in white dashed squares; scale bars: 50 μm.

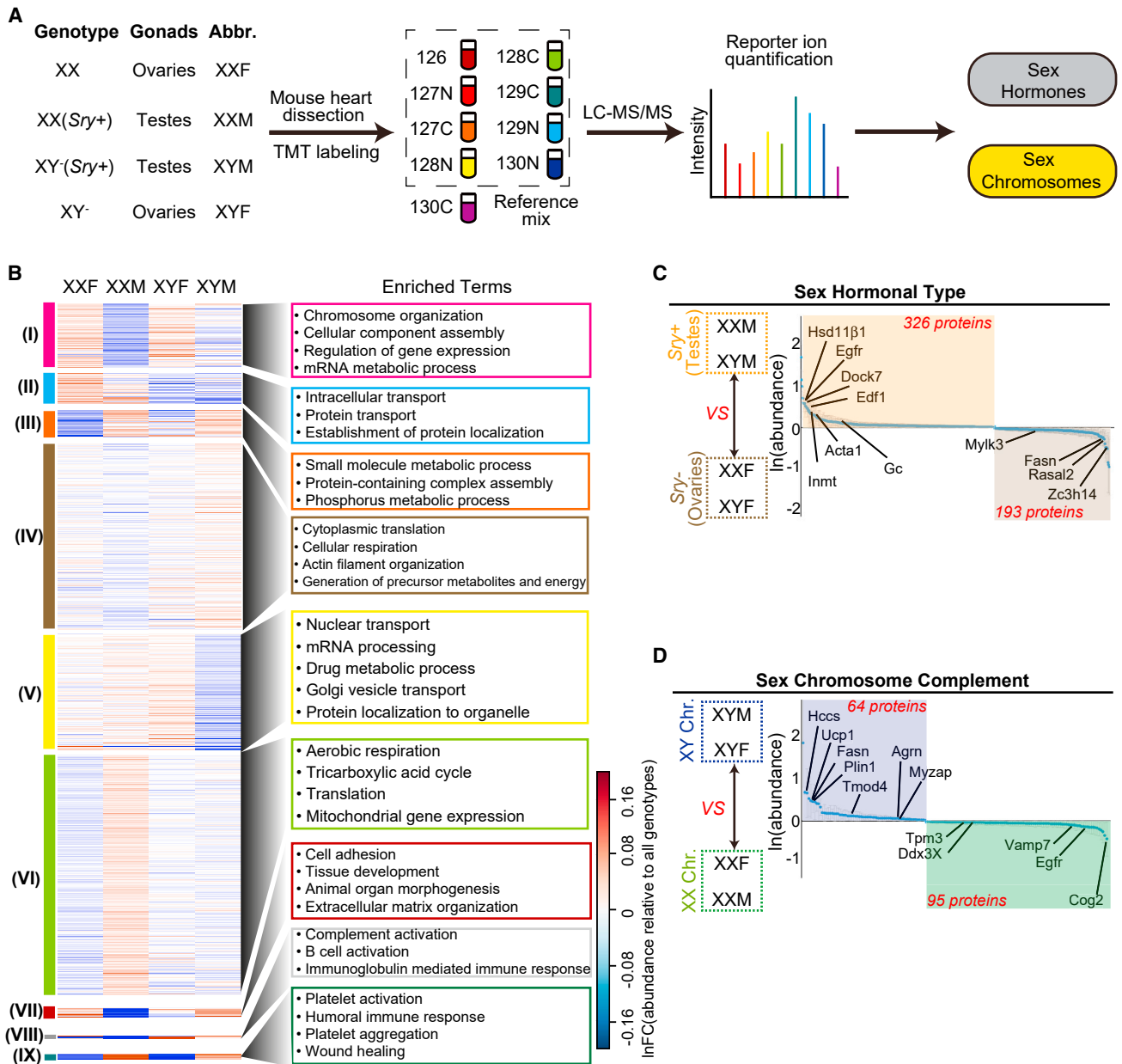See also Figures S3A–S3J and Tables S1E and S1F.

Figure 3. Cardiac proteome in the four core genotype (FCG) mouse model

(A) Design and workflow for the FCG mouse hearts; n = 3 per genotype. Abbreviations (XXF, XXM, XYM, and XYF) are used to denote each genotype hereafter. Y⁻: Y chromosome deleted for *Sry*. *Sry*+: *Sry* transgene inserted into chromosome 3.

(B) K-means clustering displayed as heatmap of identified proteins from the FCG mouse hearts. Color bar: ln (abundance relative to all genotypes). Representative enriched GO terms (FDR < 0.05, fold enrichment > 2; for clusters I–VII, protein numbers involved in each term > 10; for clusters VIII and IX, protein numbers involved in each term are > 3) in each cluster are shown in specific frames.

(C and D) Waterfall plots of differential protein abundance driven by sex-hormonal types (*Sry*+/testes [XXM and XYM] versus *Sry*⁻/ovaries [XXF and XYF]) (C) and by sex-chromosome complement (XX [XXF and XXM] versus XY [XYF and XYM]) (D) based on Bayesian inference analyses. Displayed proteins are those whose 2.5% and 97.5% quantiles of posterior distribution (central 95% Bayesian credible interval) are both greater or less than 0. The means of the posterior distribution of each protein and its credible intervals are plotted. Proteins with ln (XY/XX [or *Sry*+/*Sry*⁻] _abundance) > 0 are driven by XY chromosomes (XYM and XYF) or *Sry*+ (XXM and XYM) or otherwise driven by XX chromosomes (XXF and XXM) or *Sry*⁻ (XXF and XYF). Protein numbers are shown in each effect, and proteins of interest are labeled.

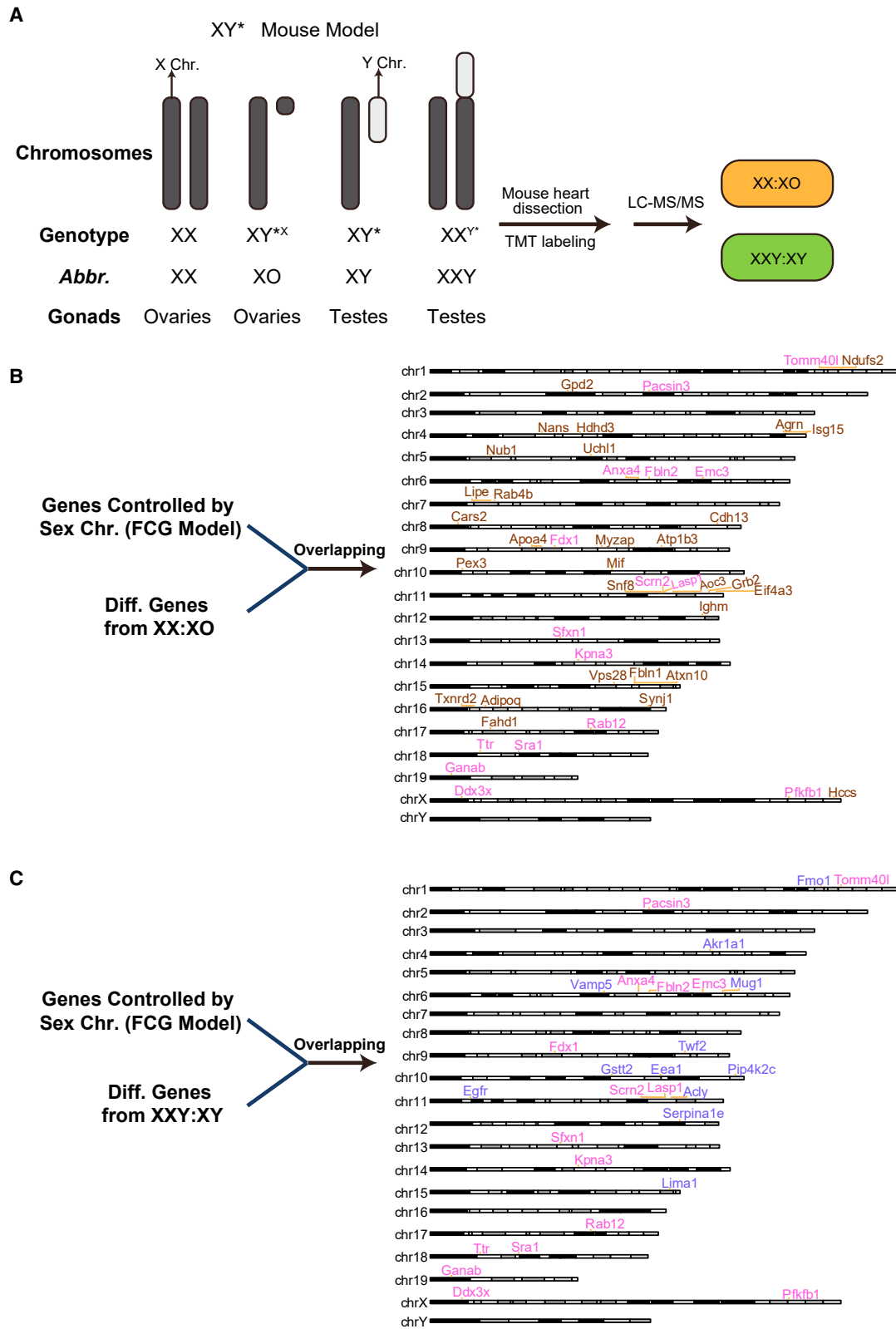See also Figures S3K–S3M and Tables S1G and S1H.

Figure 4. Differential proteins under X chromosome dosage control

(A) Design and workflow for the Turner syndrome and Klinefelter mouse hearts (n = 4 per genotype). Abbreviations (XX, XO, XY, and XXY) denote each genotype hereafter.

four FCG genotypes. K-means clustering analysis identified nine clusters of proteins that showed significant differences between at least two of the four genotypes (Figure 3B; Table S1G). Our results show that 519 proteins segregate with ovaries and testes and are thus hormonally controlled and segregate with the presence or absence of *Sry* (i.e., *Sry*-dependent) (Figure 3C; Table S1H), while 159 proteins co-segregate with sex chromosomes (XX versus XY) (Figure 3D; Table S1H). This finding confirmed the existence and function of the sex-chromosome-complement pathway in male-female cardiac tissues.

X-link proteins act in a dosage-dependent mechanism to control male-female cardiac differences

To determine if genes encoding proteins that displayed cardiac disparities are biased in their chromosomal location, we identified the human orthologs of those mouse cardiac proteins in the sex- chromosome-complement pathway. We mapped the corresponding genes to their chromosome positions in the mouse and human genome. Our results found that genes coding for the differential male-female proteins are dispersed throughout both the mouse and human genome. Surprisingly, we found that only 5% (8/159) of all cardiac proteins that had significant differences in expression between males and females mapped to genes on the mouse or human X chromosome, while none mapped to the mouse Y chromosome (Figure S4; Tables S1I and S1J).

Based on our data, we queried if X-linked genes act directly to regulate male-female differences in cardiac-protein expression by quantifying cardiac-protein abundances in heart tissue derived from XX females versus Turner syndrome females (XO) (Arnold, 2019a) (Figures 4A and S5A; Table S1K). As it is possible that reducing the number of X chromosome could lead to an alteration in gonadal hormones, we cross-referenced the Turner syndrome data with those of the sex-chromosome pathway. Analysis revealed that 30% (47/159) of cardiac proteins in the sex chromosome pathway showed altered expression in response to loss of X-linked genes (Figure 4B; Table S1L). Thus, we conclude that X-linked genes function in a dosage-sensitive mechanism to regulate cardiac-protein expression.

To determine if X-linked gene dosage is sufficient to regulate cardiac-protein expression, we quantified protein expression in heart tissue derived from XY males versus Klinefelter syndrome males (XXY) (Arnold, 2020). Cross-referencing this dataset to FCG data analyses revealed that 18% (28/159) of cardiac proteins that showed alteration in expression between XY males and XXY males takes place in the sex-chromosome-complement pathway (Figure 4C; Table S1M). Moreover, cross-referencing proteins showing a difference in XO versus XX animals, with those similarly showing a difference in XY versus XXY mice, revealed 26% (15/58) of proteins that show effects of X chromosome number (Tables S1L and S1M) that occur robustly in both gonadal females and gonadal males. These find-

ings verify that X-linked genes act outside of the gonads in a dose-dependent manner to directly control cardiac-protein expression.

Cardiac sex differences are established prior to gonad formation

CHD comprise the most common congenital malformations (Dolk et al., 2010; Heron et al., 2009). A significant portion of CHD states are developmental in origin and sex biased. To determine when, during embryogenesis, heart tissue displays sex disparities in protein expression, we took advantage of the observation that in mice, gonads do not differentiate as testes or ovaries until late in the second trimester (E11) (Garcia-Moreno et al., 2018; Nef et al., 2019), though mice have a well-formed and beating heart prior to that time (Bruneau, 2003). We set up timed mating of C57BL/6J mice, dissected hearts at E9.5 from individual embryos, and then sexed the carcasses. Proteomes of male and female hearts were determined by label-free quantitative MS (n = 3 for each sex, 20 hearts pooled per sex) (Figures 5A and S5B). A total of 7,433 proteins were quantified (Table S1N), of which 335 were found to have relatively higher levels in male E9.5 hearts and 334 in female E9.5 hearts (Figure 5B; Table S1O). As murine hearts at E9.5 are composed almost exclusively of cardiomyocytes (Bruneau, 2003), our findings would infer that the differences in male-female protein expression are, at the least in part, due to the expression of these proteins in the cardiomyocyte lineage.

We found that male-female sex biases in protein expression in adult hearts occurs principally through post-transcriptional processes. To investigate if similar mechanisms can account for male-female protein differences at E9.5, we conducted transcriptional profiling of E9.5 male and female heart tissue (Figures 5A and 5D; Table S1P). Strikingly, only 3 differential male-female cardiac proteins associated with sex-bias showed a difference at the RNA level (Figures 5A, 5B, and 5D). In aggregate, our findings imply that, as with adult heart tissue, male-female sex differences are established at E9.5 predominantly through post-transcriptional mechanisms.

To determine whether sex-biased protein expression is temporally regulated or whether it persists into adulthood, we compared our results at E9.5 (Figure 5E) with results obtained in adults and found that a small subset of proteins and cellular processes were temporally conserved; for instance, males demonstrated enhancements in proteins associated with conduction and contraction, while females demonstrated enhancements in proteins associated with metabolic processes. However, most of the cardiac sex-differentiated proteins at E9.5 displayed temporal differences by adulthood (Figure 5F). Given that our analyses were conducted prior to gonadal development, our findings strongly imply that, at this stage, male-female cardiac-protein differences are under the control of sex chromosomes. Furthermore, given that *Sry* is not expressed in

(B) X-linked genes are necessary for expression of proteins in the sex chromosome pathway. Mapping genes encoding proteins dysregulated in XX females and Turner syndrome (XO) females that overlapped with the sex-chromosome pathway. Y axis, chromosome identification. Unique genes in (B) are colored brown.
(C) X-linked genes are sufficient for proper expression of male and female cardiac proteins. Mapping genes encoding proteins dysregulated in XY males and Klinefelter syndrome (XXY) males that overlapped in the sex chromosome pathway. y axis, chromosome identification. Unique genes in (C) are colored purple. Shared genes between (B) and (C) are colored pink.
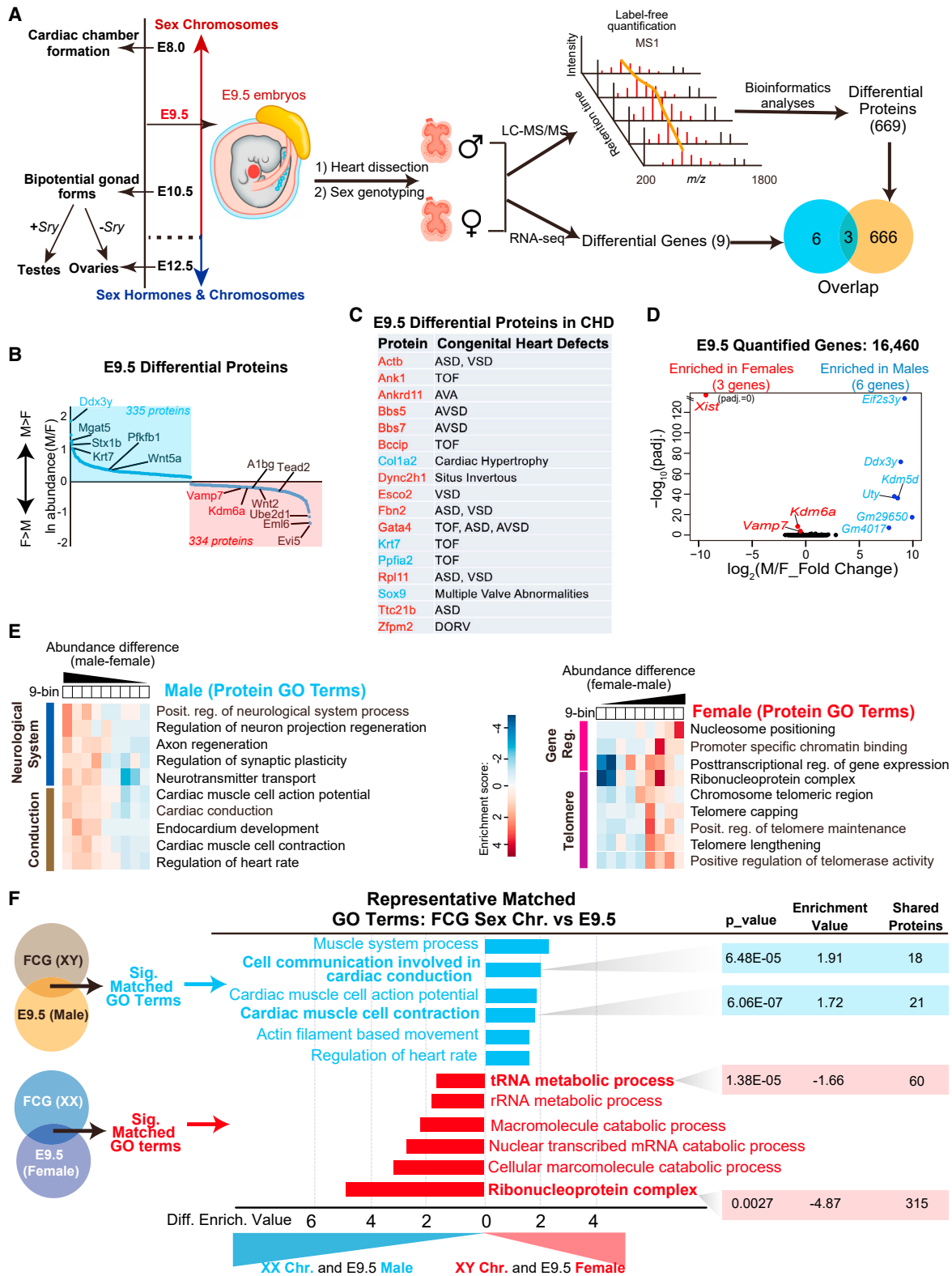See also Figures S4 and S5A and Tables S1I–S1M.

Figure 5. Cardiac proteome before sex gonad formation

(A) Design and workflow for E9.5 (n = 3 per sex, 20 hearts pooled per sex per replicate) for proteomics. Four biological replicates per sex, 6 hearts pooled as one biological replicate for RNA-seq.

(B) Waterfall plot of differential protein abundance between male and female in E9.5 embryos.

embryos prior to or at this stage (Koopman et al., 1991), our findings suggest that sex differences at E9.5 are regulated by *Sry*-independent pathways that function before gonadal development.

A1BG is required in female but not male hearts

Detailed examination of our datasets (Figure 1; Table S1B) revealed 19 of the 95 cardiac proteins showing male-female differences in protein expression to be associated with sex-biased human disease states affecting a broad range of tissue types (Table S2). In sum, 19 proteins show enrichments in processes associated with actin filament capping and actin filament-based processes (Figure S5C). We further find functional connectivity of five proteins with myosin heavy chains and an additional three of these proteins with the extra cellular matrix (ECM)/fibrinogen complex by network clustering (Figure S5D). Collectively, these data suggest a potential role for sex-biased cardiac proteins in disease states associated with ECM interactions and heart contraction.

To test the biological consequences of sex-differential proteins, we determined the requirement for the putative ECM glycoprotein A1BG in male and female hearts. We chose A1BG as a validation of our data sets as: (1) *A1bg* mRNA expression is equivalent between male and female hearts (Figures S6A and S6B); (2) A1BG is among the highest differentially expressed cardiac proteins between males and females at E9.5 and adult (Figures 1D and 5B; Tables S1B and S1N); (3) *A1bg* is encoded by an autosomal gene (chromosome 15 in mice, 19 in humans); and (4) A1BG has been proposed to interact with 3 of the 19 cardiac sex-differential proteins associated with the ECM/fibrinogen complex and human sex-bias disease state (Figure S5D; Table S2).

Analyses of our RNA-seq datasets demonstrated an equal number of reads for *A1bg* mRNA between male and female hearts (Figure S6A). Further analysis of our RNA-seq datasets showed that *A1bg* is encoded in male and female hearts by a single transcript that is identical in sequence in the coding region, the 5-UTR, and the 3-UTR and that male or female *A1bg* mRNA does not undergo alternative polyadenylation (Figure S6B). Collectively, these data show that *A1bg* mRNA is expressed at equivalent levels in male and female cardiac tissue and encoded by identical mRNA transcripts.

Analyses of single cell RNA-seq (Tabula Muris Consortium et al., 2018) demonstrates that *A1bg* mRNA is expressed at low and equivalent levels in cardiomyocytes, endothelial cells, and cardiac fibroblasts (Figure S6C). Strikingly, we find A1BG protein to be expressed at high levels in the adult left and right atrium while we observe low to undetectable levels in the ventri-

cles (Figure 6A). These results were verified by isolating adult atria and ventricles and conducting western blot analyses (n = 6 bioreplicates) (Figures S6D and S6E). Analyses of proteomic data sets from adult pigs and adult human males show similar enrichment in A1BG in the atrium versus the ventricle (Linscheid et al., 2021) (Figures 6B and 6C).

Data on E9.5 embryonic hearts (Figure 5B) and adult hearts (Figure 1D) show A1BG to be among proteins displaying significant difference in protein expression between male and female hearts. These findings were validated by western blot (Figures 6D and 6E). To further confirm that A1BG protein is expressed differentially between sexes, we quantified levels of A1BG in male and female hearts across the 8 founder strains of the CC. These data show that A1BG has dynamic expression between strains but is invariably higher in females than males both in common lab strains (A/J, C57BL/6J, NOD, and NZO) and in wild-derived strains (CAS, PWK, and WSB) (Figure 6F). We further confirmed protein-expression differences by performing targeted parallel reaction mass spectrometry (PRM-MS/MS) with six independent A1BG peptides in male and female heart tissue from C57BL/6J and NZO mouse strains. Consistent with our TMT analyses, we find that females uniformly express higher levels than males (Figures 6G, 6H, and S6F).

To test the cardiac function of A1BG, we generated cardiac conditional (Jiao et al., 2003) loss-of-function alleles of *A1bg* by CRISPR-Cas9 technologies (*Tnnt2*[cre/+];*A1bg* [flox/flox], *A1bg-KO*) (Figures 6I, S6G, and S6H). We observed that male and female mice homozygous for *A1bg-KO* were viable and born at Mendelian ratios. Strikingly, assessment of cardiac physiology revealed that female *A1bg-KO* mice have severely compromised cardiac function, which was overtly displayed as an inability of the outer left ventricle wall to properly close with the intraventricular septum during systole (Figure 6J; Videos S1, S2, S3, and S4). These physiological defects were associated with a dramatic loss in thickness of the left ventricular posterior wall (Figures 6K and 6L). In contrast, the cardiac physiology of male *A1bg-KO* mice was statistically indistinguishable from littermate controls (Figures 6K and 6L). In summary, these data establish that A1BG is required for proper cardiac function in females but not males.

DISCUSSION

Here, we performed a systems-based approach to identify quantitative molecular differences between adult and embryonic, male and female hearts. These data provide a critical resource of RNAs, proteins, protein complexes, and enriched

(C) 17 differential proteins (male versus female) at E9.5 associated with cardiac disease that display sex disparity. Blue proteins enriched in males; red proteins enriched in females. (ASD, atrial septal defects; VSD, ventricular septal defects; TOF, tetralogy of Fallot; AVA, aortic valve abnormalities; AVSD, atrioventricular septal defects; DORV, double outlet right ventricle.)

(D) Volcano plot of RNA-seq in E9.5 C57 mouse hearts showing $\log_2$ (male/female fold change) plotted against $-\log_{10}$ (padj.) determined by DESeq2. Genes $\log_2$ (male/female fold change) > 0.5 padj. < 0.05 enriched in male hearts, blue dots; $\log_2$ (male/female fold change) < −0.5, padj. < 0.05 enriched in female hearts, red dots. Representative genes in each are labeled in the plot. n = 4 per sex.

(E) Representative enriched GO terms of proteins from the E9.5 hearts. Color bar: enrichment score.

(F) Representative matched GO terms between FCG sex chromosome effect and E9.5 embryonic hearts datasets. Top 200 enriched GO terms in each dataset used to perform matching (FCG XY versus E9.5 male, FCG XX versus E9.5 female). Matched terms filtered by p value < 0.05 and abs (enrichment value) > 1.5 in E9.5 datasets; selected GO terms are defined as the significant terms, suggesting conservative control by XX or XY chromosomes in embryonic and adult stages. Representative significant terms of "FCG_XY versus E9.5 male" shown in blue, and "FCG_XX versus E9.5 female" shown in red.

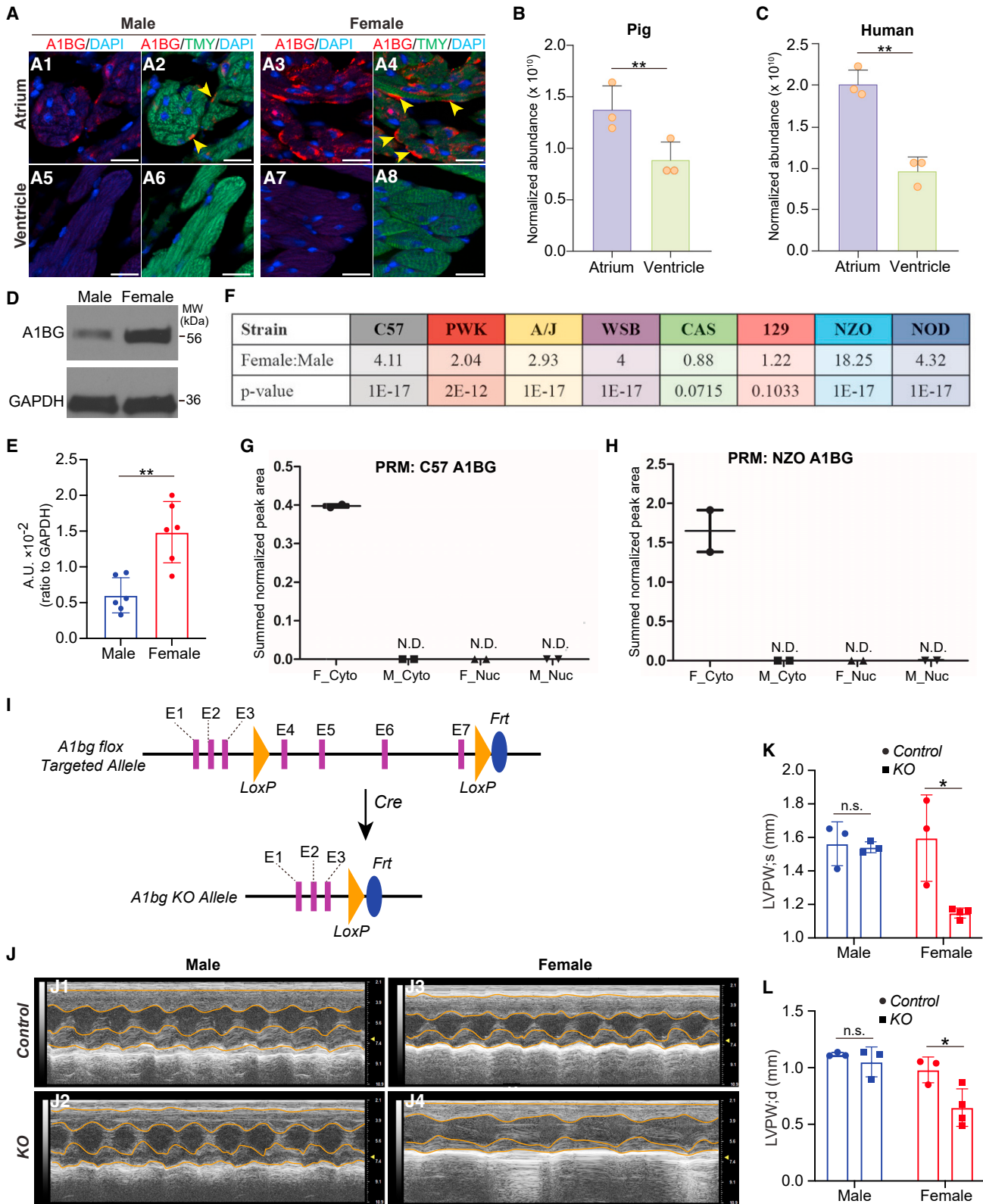See also Figure S5B and Tables S1N–S1P.

Figure 6. A1BG shows sex-biased expression patterns and function in the heart

(A) Representative IHC in adult male and female C57 heart sections. Cardiomyocytes marked by tropomyosin (green), A1BG is stained in red (arrowhead), and nucleus stained by DAPI (blue). Scale bars, 50 μm.

protein pathways for studying sex-biased cardiac disease. From our results, we would anticipate that initiating events leading to male-female differences are regulated transcriptionally and then propagated and maintained by post-transcriptional RNA mechanisms. These events in turn result in a male-female alternative translation efficiency, processing and/or protein stability that leads to sex-differential protein expression in cardiac tissues.

Cardiac sex disparities occur through hormonal and sex-chromosome mechanisms

Clinical studies and investigation into mechanisms of sex differences have challenged the paradigm that sex hormones account for all the male and female differences in prevalence, treatment, and survival of human disease. Consistent with these findings, we have used our approaches to uncover and dissect the distinct hormonal and sex chromosome pathways associated with sex differences in cardiac-protein expression. We demonstrate that, contrary to present models, male-female cardiac sex differences are not solely controlled by hormones, but rather are also controlled by sex chromosome pathways acting outside the gonads. Our data from the Turners mouse model and the Klinefelter mouse model further suggest that sex-chromosome pathways are regulated by X-linked gene dosage.

Inequalities in gene dosage from sex chromosomes is achieved by X-linked genes lacking a Y-linked homolog through escape from X-inactivation (Bellott et al., 2010; Disteche and Berletch, 2015). It is well established that a defined set of genes on the X chromosome in mouse and human escape X-inactivation in a tissue- or cell-type-specific manner (Tsuchiya and Willard, 2000; Tukiainen et al., 2018; Yang et al., 2010). Though no studies to date have defined which genes on the X chromosome escape inactivation in the heart, we note that X chromosome encoded genes *Kdm6a*, *Eif2s3x*, and *Ddx3x*, genes and proteins regulated by X-linked gene dosage in our studies, have been demonstrated to escape X-inactivation in a tissue-specific manner (Berletch et al., 2015). Our findings here would suggest that *Kdm6a*, *Eif2s3x*, and *Ddx3x* along with *Xist* itself would be candidate genes involved in initiating cardiac sex disparities.

Our data further reveal evidence that a subset of cardiac processes involve a combination of sex chromosome and gonad regulation (Figure S6I). It is possible that these pathways are regulated by both sex-chromosomal and gonadal mechanisms. Alternatively, these pathways may be driven by sex chromosome regulation, but counteracted by opposing sex hormones, thus canceling the effect of each (i.e., XYM would be equal to XXF). In the later scenario, we predict that, in disease states

involving these proteins, the patient phenotype may be similar between males and females; however, the equivalent phenotype would arise through different mechanisms in the two sexes, and hence treatment of the disease could vary between males and females.

Sex differences in cardiac-protein expression vary by strain

Here, we present quantification of proteins and cellular pathways that have been conserved and those that have diverged across the eight founder strains of the CC. CC lines were developed as an R1 resource panel for quantitative trait locus (QTL) mapping, and more than 60 CC strains are commercially available. Since all CC strains are inbred (and genetically identical) and their genomes fully sequenced, they are a highly reproducible resource for loci mapping (Chesler et al., 2008; Chick et al., 2016; Churchill et al., 2004; Morgan and Welsh, 2015; Saul et al., 2019; Sigmon et al., 2020; Threadgill and Churchill, 2012; Threadgill et al., 2011). These attributes have proven extremely powerful in mapping QTLs such as susceptibility loci to infectious disease, viral infection, and glucose intolerance (Abu Toamih Atamni et al., 2018, 2019; Brinkmeyer-Langford et al., 2017; Kollmus et al., 2018; Manet et al., 2020). Thus, data presented here will additionally allow selection of the appropriate founder strains for QTL mapping of male-female differentially regulated proteins involved in cardiac disease. In addition, given the well-established recognition of sex differences in cardiac surgical models (Doetschman, 2009; Fontaine and Davis, 2016; Hunter, 2012), our results will also provide a community resource enabling the selection of the best mouse strains *a priori* for any given model.

Sex differences in the cardiomyocyte lineage are established prior to gonad formation

CHD is the most prevalent and lethal cause of birth defects in the US and Europe (Dolk et al., 2010; Heron et al., 2009). A significant portion of these disease states are sex biased (Garcia et al., 2016; Haberer and Silversides, 2019; Prabhavathi et al., 2014). Our findings demonstrate that the onset of sex-biased protein expression in cardiomyocytes occurs at the earliest stages of heart development; a period shortly after cardiomyocyte fate is determined and prior to gonad formation. These findings are broadly consistent with studies that show sex-biased expression of transcription and epigenetic factors are maintained during differentiation of embryonic stem cells into cardiac precursors (Werner et al., 2017). Of the proteins we found differentially regulated among males and females at E9.5, 17 were associated with

(B and C) Normalized abundance of A1BG protein in pig (B) and human (C) atrium and ventricle. (Data from Linscheid et al., 2021). (n = 3 per tissue; **p < 0.01; error bars represent mean ± SEM.)

(D and E) Western blot (D) and quantification (E) of protein abundance of A1BG in male and female mouse hearts. (n = 6 per sex; **p < 0.01; error bars represent mean ± SEM.) Data represented relative to GAPDH.

(F) Differential expression of A1BG between male and female hearts in all 8 founders.

(G and H) Quantification of peptides with normalized intensity. Coefficient of variance < 20% in the PRM assay of C57 (G) and NZO (H) mouse heart samples (n = 2 per sex per cellular fraction).

(I) Gene targeting strategy to generate conditional *A1bg-KO* line.

(J) Representative examples of M-mode echocardiography of male and female *A1bg-KO* (*Tnnt2*$^{Cre/+}$;*A1bg*$^{flox/flox}$) and control (*A1bg* $^{flox/flox}$) mouse hearts.

(K and L) Quantification of end-systolic posterior wall thickness (LVPWs; K) or end-diastolic posterior wall thickness (LVPWd; L) of male and female *A1bg-KO* and control mouse hearts (n = 3–4 per sex per genotype; *p < 0.05, error bars represent mean ± SD).

See also Figure S6.

congenital cardiac disease states that display sex disparity (Figure 5C). However, we have found no reports of these proteins displaying sex differences in expression during development. Five of these proteins are encoded by genes known to cause tetralogy of Fallot (TOF), a severe congenital heart defect that, even when taking risk factors into account, preferentially effects males: *Krt7*, *Bccip*, *Ank1*, *Ppfia2*, and *Gata4* (Jin et al., 2017; Lahm et al., 2015). The finding that GATA4, an extensively studied cardiac transcription factor, is upregulated in female E9.5 hearts is of additional clinical importance, given that mutations in *Gata4* are also causally associated with two other prevalent sex-biased disease states: atrial septal defects and atrioventricular septal defects (Zhou et al., 2017).

Sex-biased requirement for A1BG in cardiac function

Here, we demonstrated the power and utility of our datasets by showing a sex-disparate function for A1BG (Figure 6). Female mice with conditional loss-of-function *A1bg* alleles display anatomical and physiological cardiac dysfunction while male mice do not. These findings indicate an essential requirement for A1BG in females while A1BG appears to be dispensable in males. This conclusion is in line with our findings that A1BG is expressed at undetectable levels in adult wild-type NZO male hearts (Figure 6H). Notably, NZO mice are widely reported to have a sex disparity in obesity with male, but not female mice, displaying dramatic weight gain, development of associated diabetes, and compromised cardiac function (John et al., 2018; Jürgens et al., 2006; Petkov et al., 2004). From these findings, we propose that A1BG acts to mediate a cardiac-stress response upon obesity, injury, or hypoxia. As A1BG is expressed in human hearts (Linscheid et al., 2021), it will be of great interest to explore the relationship between A1BG in human obesity and cardiac function.

Limitations of the study

Our findings imply that cardiac sex differences are initiated by X-linked genes that act via a dosage-specific mechanism. Testing this hypothesis and identifying the genes on the X chromosome that initiate sex disparities in a cardiac-specific manner will be influential in understanding how X-linked genes function in a tissue-specific manner outside the gonads.

In the future it will be critical to determine if these mechanisms not only regulate male-female cardiac differences but also apply to the sex disparities observed in many other disease states, including cancer, dementia, chronic kidney disease, obesity, and autoimmune disease (Babapour Mofrad and van der Flier, 2019; Channappanavar et al., 2017; Christou et al., 2019; Kadioglu et al., 2011; Leung, 2020; Liang et al., 2017; Luders et al., 2009; Snell and Turner, 2018; Zhu et al., 2000).

STAR★METHODS

Detailed methods are provided in the online version of this paper and include the following:

- KEY RESOURCES TABLE
- RESOURCE AVAILABILITY
  - Lead contact
  - Materials availability
  - Data and code availability
- EXPERIMETAL MODEL AND SUBJECT DETAILS
  - Mouse
- METHOD DETAILS
  - RNA-sequencing analysis
  - Dissection and sex genotyping of E9.5 embryonic hearts
  - Immunohistochemistry
  - Western blot
  - Generation of cardiac A1bg knockout mouse
  - Echocardiography
  - Mass spectrometry sample preparation
  - Peptide fractionation
  - Parallel reaction monitoring (PRM) sample preparation
  - PRM LC-MS/MS analysis
- QUANTIFICATION AND STATISTICAL ANALYSIS
  - Mass spectrometry analyses
  - Database searching and reporter ion quantitation or label-free quantitation
  - Gene set enrichment analyses
  - Bayesian inference analysis
  - PRM data analysis

REFERENCES

Abu Toamih Atamni, H., Nashef, A., and Iraqi, F.A. (2018). The Collaborative cross mouse model for dissecting genetic susceptibility to infectious diseases. Mamm. Genome *29*, 471–487.

Abu-Toamih Atamni, H.J., Kontogianni, G., Binenbaum, I., Mott, R., Himmelbauer, H., Lehrach, H., Chatziioannou, A., and Iraqi, F.A. (2019). Hepatic gene expression variations in response to high-fat diet-induced impaired glucose tolerance using RNAseq analysis in collaborative cross mouse population. Mamm. Genome *30*, 260–275.

Arnold, A.L., Milner, K.A., and Vaccarino, V. (2001). Sex and race differences in electrocardiogram use (the National Hospital Ambulatory Medical Care Survey). Am. J. Cardiol. *88*, 1037–1040.

Arnold, A.P. (2017). Y chromosome's roles in sex differences in disease. Proc. Natl. Acad. Sci. USA *114*, 3787–3789.

Arnold, A.P. (2019a). The mouse as a model of fundamental concepts related to Turner syndrome. Am. J. Med. Genet. C Semin. Med. Genet. *181*, 76–85.

Arnold, A.P. (2019b). Rethinking sex determination of non-gonadal tissues. Curr. Top. Dev. Biol. *134*, 289–315.

Arnold, A.P. (2020). Four core genotypes and XY* mouse models: update on impact on SABV research. Neurosci. Biobehav. Rev. *119*, 1–8.

Arnold, A.P., Cassis, L.A., Eghbali, M., Reue, K., and Sandberg, K. (2017). Sex hormones and sex chromosomes cause sex differences in the development of cardiovascular diseases. Arterioscler. Thromb. Vasc. Biol. *37*, 746–756.

Babapour Mofrad, R., and van der Flier, W.M. (2019). Nature and implications of sex differences in AD pathology. Nat. Rev. Neurol. *15*, 6–8.

Bellott, D.W., Skaletsky, H., Pyntikova, T., Mardis, E.R., Graves, T., Kremitzki, C., Brown, L.G., Rozen, S., Warren, W.C., Wilson, R.K., and Page, D.C. (2010). Convergent evolution of chicken Z and human X chromosomes by expansion and gene acquisition. Nature *466*, 612–616.

Berletch, J.B., Ma, W., Yang, F., Shendure, J., Noble, W.S., Disteche, C.M., and Deng, X. (2015). Escape from X inactivation varies in mouse tissues. PLoS Genet *11*, e1005079.

Blenck, C.L., Harvey, P.A., Reckelhoff, J.F., and Leinwand, L.A. (2016). The importance of biological sex and estrogen in rodent models of cardiovascular health and disease. Circ. Res. *118*, 1294–1312.

Böhm, C., Benz, V., Clemenz, M., Sprang, C., Höft, B., Kintscher, U., and Foryst-Ludwig, A. (2013). Sexual dimorphism in obesity-mediated left ventricular hypertrophy. Am. J. Physiol. Heart Circ. Physiol. *305*, H211–H218.

Brennan, J., and Capel, B. (2004). One tissue, two fates: molecular genetic events that underlie testis versus ovary development. Nat. Rev. Genet. *5*, 509–521.

Brinkmeyer-Langford, C.L., Rech, R., Amstalden, K., Kochan, K.J., Hillhouse, A.E., Young, C., Welsh, C.J., and Threadgill, D.W. (2017). Host genetic background influences diverse neurological responses to viral infection in mice. Sci. Rep. *7*, 12194.

Bruneau, B.G. (2003). The developing heart and congenital heart defects: a make or break situation. Clin. Genet. *63*, 252–261.

Burgoyne, P.S., and Arnold, A.P. (2016). A primer on the use of mouse models for identifying direct sex chromosome effects that cause sex differences in non-gonadal tissues. Biol. Sex Differ. *7*, 68.

Channappanavar, R., Fett, C., Mack, M., Ten Eyck, P.P., Meyerholz, D.K., and Perlman, S. (2017). Sex-based differences in susceptibility to severe acute respiratory syndrome coronavirus infection. J. Immunol. *198*, 4046–4053.

Chesler, E.J., Miller, D.R., Branstetter, L.R., Galloway, L.D., Jackson, B.L., Philip, V.M., Voy, B.H., Culiat, C.T., Threadgill, D.W., Williams, R.W., et al. (2008). The Collaborative Cross at Oak Ridge National Laboratory: developing a powerful resource for systems genetics. Mamm. Genome *19*, 382–389.

Chester, R.C., Kling, J.M., and Manson, J.E. (2018). What the Women's Health Initiative has taught us about menopausal hormone therapy. Clin. Cardiol. *41*, 247–252.

Chick, J.M., Munger, S.C., Simecek, P., Huttlin, E.L., Choi, K., Gatti, D.M., Raghupathy, N., Svenson, K.L., Churchill, G.A., and Gygi, S.P. (2016). Defining the consequences of genetic variation on a proteome-wide scale. Nature *534*, 500–505.

Chlebowski, R.T., Barrington, W., Aragaki, A.K., Manson, J.E., Sarto, G., O'Sullivan, M.J., Wu, D., Cauley, J.A., Qi, L., Wallace, R.L., and Prentice, R.L. (2017). Estrogen alone and health outcomes in black women by African ancestry: a secondary analyses of a randomized controlled trial. Menopause *24*, 133–141.

Christou, E.A.A., Banos, A., Kosmara, D., Bertsias, G.K., and Boumpas, D.T. (2019). Sexual dimorphism in SLE: above and beyond sex hormones. Lupus *28*, 3–10.

Churchill, G.A., Airey, D.C., Allayee, H., Angel, J.M., Attie, A.D., Beatty, J., Beavis, W.D., Belknap, J.K., Bennett, B., Berrettini, W., et al. (2004). The Collaborative Cross, a community resource for the genetic analysis of complex traits. Nat. Genet. *36*, 1133–1137.

Dent, M.R., Tappia, P.S., and Dhalla, N.S. (2011). Gender differences in beta-adrenoceptor system in cardiac hypertrophy due to arteriovenous fistula. J. Cell. Physiol. *226*, 181–186.

Dieseldorff Jones, K.M., Vied, C., Valera, I.C., Chase, P.B., Parvatiyar, M.S., and Pinto, J.R. (2020). Sexual dimorphism in cardiac transcriptome associated with a troponin C murine model of hypertrophic cardiomyopathy. Physiol. Rep. *8*, e14396.

Disteche, C.M., and Berletch, J.B. (2015). X chromosome inactivation and escape. J. Genet. *94*, 591–599.

Doetschman, T. (2009). Influence of genetic background on genetically engineered mouse phenotypes. Methods Mol. Biol. *530*, 423–433.

Dolk, H., Loane, M., and Garne, E. (2010). The prevalence of congenital anomalies in Europe. Adv. Exp. Med. Biol. *686*, 349–364.

Dorr, K.M., Amin, N.M., Kuchenbrod, L.M., Labiner, H., Charpentier, M.S., Pevny, L.H., Wessels, A., and Conlon, F.L. (2015). Casz1 is required for cardiomyocyte G1-to-S phase progression during mammalian cardiac development. Development *142*, 2037–2047.

Federspiel, J.D., Tandon, P., Wilczewski, C.M., Wasson, L., Herring, L.E., Venkatesh, S.S., Cristea, I.M., and Conlon, F.L. (2019). Conservation and divergence of protein pathways in the vertebrate heart. PLoS Biol *17*, e3000437.

Fiedler, L.R., Chapman, K., Xie, M., Maifoshie, E., Jenkins, M., Golforoush, P.A., Bellahcene, M., Noseda, M., Faust, D., Jarvis, A., et al. (2020). MAP4K4 inhibition promotes survival of human stem cell-derived cardiomyocytes and reduces infarct size in vivo. Cell Stem Cell *26*, 458.

Fontaine, D.A., and Davis, D.B. (2016). Attention to background strain is essential for metabolic research: C57BL/6 and the international knockout mouse consortium. Diabetes *65*, 25–33.

Garcia, M., Mulvagh, S.L., Merz, C.N., Buring, J.E., and Manson, J.E. (2016). Cardiovascular disease in women: clinical perspectives. Circ. Res. *118*, 1273–1293.

Garcia-Moreno, S.A., Plebanek, M.P., and Capel, B. (2018). Epigenetic regulation of male fate commitment from an initially bipotential system. Mol. Cell. Endocrinol. *468*, 19–30.

Giannakoulas, G., Vasiliadis, K., Frogoudaki, A., Ntellos, C., Tzifa, A., Brili, S., Manginas, A., Papaphylactou, M., Parcharidou, D., Kampouridis, N., et al. (2017). Adult congenital heart disease in Greece: preliminary data from the CHALLENGE registry. Int. J. Cardiol. *245*, 109–113.

Goodarzi, H., Elemento, O., and Tavazoie, S. (2009). Revealing global regulatory perturbations across human cancers. Mol. Cell *36*, 900–911.

Haberer, K., and Silversides, C.K. (2019). Congenital heart disease and women's health across the life span: focus on reproductive issues. Can. J. Cardiol. *35*, 1652–1663.

Harrington, J., Fillmore, N., Gao, S., Yang, Y., Zhang, X., Liu, P., Stoehr, A., Chen, Y., Springer, D., Zhu, J., et al. (2017). A systems biology approach to investigating sex differences in cardiac hypertrophy. J. Am. Heart Assoc. *6*, e005838.

Heron, M., Hoyert, D.L., Murphy, S.L., Xu, J., Kochanek, K.D., and Tejada-Vera, B. (2009). Deaths: final data for 2006. Natl. Vital Stat. Rep. *57*, 1–134.

Homburger, J.R., Green, E.M., Caleshu, C., Sunitha, M.S., Taylor, R.E., Ruppel, K.M., Metpally, R.P., Colan, S.D., Michels, M., Day, S.M., et al. (2016). Multidimensional structure-function relationships in human beta-cardiac myosin from population-scale genetic variation. Proc. Natl. Acad. Sci. USA *113*, 6701–6706.

Hunter, K.W. (2012). Mouse models of cancer: does the strain matter? Nat. Rev. Cancer *12*, 144–149.

Jiao, K., Kulessa, H., Tompkins, K., Zhou, Y., Batts, L., Baldwin, H.S., and Hogan, B.L. (2003). An essential role of Bmp4 in the atrioventricular septation of the mouse heart. Genes Dev *17*, 2362–2367.

Jin, S.C., Homsy, J., Zaidi, S., Lu, Q., Morton, S., DePalma, S.R., Zeng, X., Qi, H., Chang, W., Sierant, M.C., et al. (2017). Contribution of rare inherited and de novo variants in 2,871 congenital heart disease probands. Nat. Genet. *49*, 1593–1601.

John, C., Grune, J., Ott, C., Nowotny, K., Deubel, S., Kühne, A., Schubert, C., Kintscher, U., Regitz-Zagrosek, V., and Grune, T. (2018). Sex differences in cardiac mitochondria in the New Zealand obese mouse. Front. Endocrinol. (Lausanne) *9*, 732.

Jordan, P., Gonçalves, V., Fernandes, S., Marques, T., Pereira, M., and Gama-Carvalho, M. (2019). Networks of mRNA processing and alternative splicing regulation in health and disease. Adv. Exp. Med. Biol. *1157*, 1–27.

Jürgens, H.S., Schürmann, A., Kluge, R., Ortmann, S., Klaus, S., Joost, H.G., and Tschöp, M.H. (2006). Hyperphagia, lower body temperature, and reduced running wheel activity precede development of morbid obesity in New Zealand obese mice. Physiol. Genomics *25*, 234–241.

Kadioglu, A., Cuppone, A.M., Trappetti, C., List, T., Spreafico, A., Pozzi, G., Andrew, P.W., and Oggioni, M.R. (2011). Sex-based differences in susceptibility to respiratory and systemic pneumococcal disease in mice. J. Infect. Dis. *204*, 1971–1979.

Kararigas, G., Dworatzek, E., Petrov, G., Summer, H., Schulze, T.M., Baczko, I., Knosalla, C., Golz, S., Hetzer, R., and Regitz-Zagrosek, V. (2014). Sex-dependent regulation of fibrosis and inflammation in human left ventricular remodelling under pressure overload. Eur. J. Heart Fail. *16*, 1160–1167.

Kennedy, L., Kaltenbrun, E., Greco, T.M., Temple, B., Herring, L.E., Cristea, I.M., and Conlon, F.L. (2017). Formation of a TBX20-CASZ1 protein complex is protective against dilated cardiomyopathy and critical for cardiac homeostasis. PLoS Genet. *13*, e1007011.

Kollmus, H., Pilzner, C., Leist, S.R., Heise, M., Geffers, R., and Schughart, K. (2018). Of mice and men: the host response to influenza virus infection. Mamm. Genome *29*, 446–470.

Konhilas, J.P., Chen, H., Luczak, E., McKee, L.A., Regan, J., Watson, P.A., Stauffer, B.L., Khalpey, Z.I., Mckinsey, T.A., Horn, T., et al. (2015). Diet and sex modify exercise and cardiac adaptation in the mouse. Am. J. Physiol. Heart Circ. Physiol. *308*, H135–H145.

Koopman, P., Gubbay, J., Vivian, N., Goodfellow, P., and Lovell-Badge, R. (1991). Male development of chromosomally female mice transgenic for Sry. Nature *351*, 117–121.

Lahm, H., Schön, P., Doppler, S., Dreßen, M., Cleuziou, J., Deutsch, M.A., Ewert, P., Lange, R., and Krane, M. (2015). Tetralogy of Fallot and hypoplastic left heart syndrome - complex clinical phenotypes meet complex genetic networks. Curr. Genomics *16*, 141–158.

Leung, C. (2020). Clinical features of deaths in the novel coronavirus epidemic in China. Rev. Med. Virol. *30*, e2103.

Liang, Y., Tsoi, L.C., Xing, X., Beamer, M.A., Swindell, W.R., Sarkar, M.K., Berthier, C.C., Stuart, P.E., Harms, P.W., Nair, R.P., et al. (2017). A gene network regulated by the transcription factor VGLL3 as a promoter of sex-biased autoimmune diseases. Nat. Immunol. *18*, 152–160.

Linscheid, N., Santos, A., Poulsen, P.C., Mills, R.W., Calloe, K., Leurs, U., Ye, J.Z., Stolte, C., Thomsen, M.B., Bentzen, B.H., et al. (2021). Quantitative proteome comparison of human hearts with those of model organisms. PLoS Biol *19*, e3001144.

Luders, E., Gaser, C., Narr, K.L., and Toga, A.W. (2009). Why sex matters: brain size independent differences in gray matter distributions between men and women. J. Neurosci. *29*, 14265–14270.

Manet, C., Simon-Lorière, E., Jouvion, G., Hardy, D., Prot, M., Conquet, L., Flamand, M., Panthier, J.J., Sakuntabhai, A., and Montagutelli, X. (2020). Genetic diversity of collaborative cross mice controls viral replication, clinical severity, and brain pathology induced by Zika virus infection. independently of Oas1b. J. Virol. *94*, e01034–19.

Marian, A.J., and Braunwald, E. (2017). Hypertrophic cardiomyopathy: genetics, pathogenesis, clinical manifestations, diagnosis, and therapy. Circ. Res. *121*, 749–770.

Maric-Bilkan, C., Arnold, A.P., Taylor, D.A., Dwinell, M., Howlett, S.E., Wenger, N., Reckelhoff, J.F., Sandberg, K., Churchill, G., Levin, E., and Lundberg, M.S. (2016). Report of the National Heart, Lung, and Blood Institute working group on sex differences research in cardiovascular disease: scientific questions and challenges. Hypertension *67*, 802–807.

Morgan, A.P., and Welsh, C.E. (2015). Informatics resources for the Collaborative Cross and related mouse populations. Mamm. Genome *26*, 521–539.

Morita, H., Rehm, H.L., Menesses, A., McDonough, B., Roberts, A.E., Kucherlapati, R., Towbin, J.A., Seidman, J.G., and Seidman, C.E. (2008). Shared genetic causes of cardiac hypertrophy in children and adults. N. Engl. J. Med. *358*, 1899–1908.

Mosca, L., Banka, C.L., Benjamin, E.J., Berra, K., Bushnell, C., Dolor, R.J., Ganiats, T.G., Gomes, A.S., Gornik, H.L., Gracia, C., et al. (2007). Evidence-based guidelines for cardiovascular disease prevention in women: 2007 update. J. Am. Coll. Cardiol. *49*, 1230–1250.

Mosca, L., Barrett-Connor, E., and Wenger, N.K. (2011a). Sex/gender differences in cardiovascular disease prevention: what a difference a decade makes. Circulation *124*, 2145–2154.

Mosca, L., Benjamin, E.J., Berra, K., Bezanson, J.L., Dolor, R.J., Lloyd-Jones, D.M., Newby, L.K., Piña, I.L., Roger, V.L., Shaw, L.J., et al. (2011b). Effectiveness-based guidelines for the prevention of cardiovascular disease in women–2011 update: a guideline from the American Heart Association. J. Am. Coll. Cardiol. *57*, 1404–1423.

Naqvi, S., Godfrey, A.K., Hughes, J.F., Goodheart, M.L., Mitchell, R.N., and Page, D.C. (2019). Conservation, acquisition, and functional impact of sex-biased gene expression in mammals. Science *365*, eaaw7317.

Nef, S., Stévant, I., and Greenfield, A. (2019). Characterizing the bipotential mammalian gonad. Curr. Top. Dev. Biol. *134*, 167–194.

Olivotto, I., Maron, M.S., Adabag, A.S., Casey, S.A., Vargiu, D., Link, M.S., Udelson, J.E., Cecchi, F., and Maron, B.J. (2005). Gender-related differences in the clinical presentation and outcome of hypertrophic cardiomyopathy. J. Am. Coll. Cardiol. *46*, 480–487.

ORIGIN Trial Investigators, Gerstein, H.C., Bosch, J., Dagenais, G.R., Díaz, R., Jung, H., Maggioni, A.P., Pogue, J., Probstfield, J., Ramachandran, A., et al. (2012). Basal insulin and cardiovascular and other outcomes in dysglycemia. N. Engl. J. Med. *367*, 319–328.

Patrizio, M., and Marano, G. (2016). Gender differences in cardiac hypertrophic remodeling. Ann. Ist. Super. Sanita. *52*, 223–229.

Peters, S.A.E., Muntner, P., and Woodward, M. (2019). Sex differences in the prevalence of, and trends in, cardiovascular risk factors, treatment, and control in the United States, 2001 to 2016. Circulation *139*, 1025–1035.

Petkov, P.M., Cassell, M.A., Sargent, E.E., Donnelly, C.J., Robinson, P., Crew, V., Asquith, S., Haar, R.V., and Wiles, M.V. (2004). Development of a SNP genotyping panel for genetic monitoring of the laboratory mouse. Genomics *83*, 902–911.

Prabhavathi, K., Selvi, K.T., Poornima, K.N., and Sarvanan, A. (2014). Role of biological sex in normal cardiac function and in its disease outcome - a review. J. Clin. Diagn. Res. *8*, BE01–BE04.

Queirós, A.M., Eschen, C., Fliegner, D., Kararigas, G., Dworatzek, E., Westphal, C., Sanchez Ruderisch, H., and Regitz-Zagrosek, V. (2013). Sex- and estrogen-dependent regulation of a miRNA network in the healthy and hypertrophied heart. Int. J. Cardiol. *169*, 331–338.

Rappsilber, J., Mann, M., and Ishihama, Y. (2007). Protocol for micro-purification, enrichment, pre-fractionation and storage of peptides for proteomics using StageTips. Nat. Protoc. *2*, 1896–1906.

Regitz-Zagrosek, V., and Kararigas, G. (2017). Mechanistic pathways of sex differences in cardiovascular disease. Physiol. Rev. *97*, 1–37.

Regitz-Zagrosek, V., and Seeland, U. (2011). Sex and gender differences in myocardial hypertrophy and heart failure. Wien. Med. Wochenschr. *161*, 109–116.

Rosa-Caldwell, M.E., and Greene, N.P. (2019). Muscle metabolism and atrophy: let's talk about sex. Biol. Sex Differ. *10*, 43.

Sabater-Molina, M., Pérez-Sánchez, I., Hernández Del Rincón, J.P., and Gimeno, J.R. (2018). Genetics of hypertrophic cardiomyopathy: a review of current state. Clin. Genet. *93*, 3–14.

San Roman, A.K., and Page, D.C. (2019). A strategic research alliance: Turner syndrome and sex differences. Am. J. Med. Genet. C Semin. Med. Genet. *181*, 59–67.

Saul, M.C., Philip, V.M., Reinholdt, L.G.; Center for Systems Neurogenetics of Addiction, and Chesler, E.J. (2019). High-diversity mouse populations for complex traits. Trends Genet. *35*, 501–514.

Shioura, K.M., Geenen, D.L., and Goldspink, P.H. (2008). Sex-related changes in cardiac function following myocardial infarction in mice. Am. J. Physiol. Regul. Integr. Comp. Physiol. *295*, R528–R534.

Sigmon, J.S., Blanchard, M.W., Baric, R.S., Bell, T.A., Brennan, J., Brockmann, G.A., Burks, A.W., Calabrese, J.M., Caron, K.M., Cheney, R.E., et al. (2020). Content and performance of the MiniMUGA genotyping array: a new tool to improve rigor and reproducibility in mouse research. Genetics *216*, 905–930.

Snell, D.M., and Turner, J.M.A. (2018). Sex chromosome effects on male-female differences in mammals. Curr. Biol. *28*, R1313–R1324.

Tabula Muris Consortium; Overall coordination; Logistical coordination; Organ collection and processing; Library preparation and sequencing; Computational data analysis; Cell type annotation; Writing group; Supplemental text writing group; Principal investigators (2018). Single-cell transcriptomics of 20 mouse organs creates a Tabula Muris. Nature *562*, 367–372.

Threadgill, D.W., and Churchill, G.A. (2012). Ten years of the Collaborative Cross. Genetics *190*, 291–294.

Threadgill, D.W., Miller, D.R., Churchill, G.A., and de Villena, F.P.-M. (2011). The collaborative cross: a recombinant inbred mouse population for the systems genetic era. ILAR J. *52*, 24–31.

Tsuchiya, K.D., and Willard, H.F. (2000). Chromosomal domains and escape from X inactivation: comparative X inactivation analysis in mouse and human. Mamm. Genome *11*, 849–854.

Tukiainen, T., Villani, A.-C., Yen, A., Rivas, M.A., Marshall, J.L., Satija, R., Aguirre, M., Gauthier, L., Fleharty, M., Kirby, A., et al. (2018). Corrigendum: landscape of X chromosome inactivation across human tissues. Nature *555*, 274.

Ventura-Clapier, R., Dworatzek, E., Seeland, U., Kararigas, G., Arnal, J.-F., Brunelleschi, S., Carpenter, T.C., Erdmann, J., Franconi, F., Giannetta, E., et al. (2017). Sex in basic research: concepts in the cardiovascular field. Cardiovasc. Res. *113*, 711–724.

Werner, R.J., Schultz, B.M., Huhn, J.M., Jelinek, J., Madzo, J., and Engel, N. (2017). Sex chromosomes drive gene expression and regulatory dimorphisms in mouse embryonic stem cells. Biol. Sex Differ. *8*, 28.

Whayne, T.F., Jr., and Mukherjee, D. (2015). Women, the menopause, hormone replacement therapy and coronary heart disease. Curr. Opin. Cardiol. *30*, 432–438.

Wilczewski, C.M., Hepperla, A.J., Shimbo, T., Wasson, L., Robbe, Z.L., Davis, I.J., Wade, P.A., and Conlon, F.L. (2018). CHD4 and the NuRD complex directly control cardiac sarcomere formation. Proc. Natl. Acad. Sci. USA *115*, 6727–6732.

Witt, H., Schubert, C., Jaekel, J., Fliegner, D., Penkalla, A., Tiemann, K., Stypmann, J., Roepcke, S., Brokat, S., Mahmoodzadeh, S., et al. (2008). Sex-specific pathways in early cardiac response to pressure overload in mice. J. Mol. Med. (Berl.) *86*, 1013–1024.

Wu, J., Dai, F., Li, C., and Zou, Y. (2020). Gender differences in cardiac hypertrophy. J. Cardiovasc. Transl. Res. *13*, 73–84.

Wu, J.C., Nasseri, B.A., Bloch, K.D., Picard, M.H., and Scherrer-Crosbie, M. (2003). Influence of sex on ventricular remodeling after myocardial infarction in mice. J. Am. Soc. Echocardiogr. *16*, 1158–1162.

Yang, F., Babak, T., Shendure, J., and Disteche, C.M. (2010). Global survey of escape from X inactivation by RNA-sequencing in mouse. Genome Res *20*, 614–622.

Zhou, L., Liu, J., Xiang, M., Olson, P., Guzzetta, A., Zhang, K., Moskowitz, I.P., and Xie, L. (2017). Gata4 potentiates second heart field proliferation and Hedgehog signaling for cardiac septation. Proc. Natl. Acad. Sci. USA *114*, E1422–E1431.

Zhu, J., Shearer, G.M., Norman, J.E., Pinto, L.A., Marincola, F.M., Prasad, A., Waclawiw, M.A., Csako, G., Quyyumi, A.A., and Epstein, S.E. (2000). Host response to cytomegalovirus infection as a determinant of susceptibility to coronary artery disease: sex-based differences in inflammation and type of immune response. Circulation *102*, 2491–2496.

STAR★METHODS

KEY RESOURCES TABLE

REAGENT or RESOURCE	SOURCE	IDENTIFIER
Antibodies		
Rabbit monoclonal anti-Emerin (Emd)	Abcam	Cat# ab156871
Rabbit polyclonal anti-Dystrophin (Dmd)	Abcam	Cat# ab15277; RRID: AB_301813
Rabbit polyclonal anti-Atrx	Abcam	Cat# ab97508; RRID: AB_10680289
Rabbit polyclonal anti-A1bg	Abcam	Cat# Ab231805
Rabbit polyclonal anti-A1bg	Sigma	Cat# HPA044252; RRID: AB_2678876
Rabbit polyclonal anti-Ddx3	Abcam	Cat# ab235940
Rabbit polyclonal anti-Pbdc1	Sigma	Cat# HPA003155; RRID: AB_1078592
Mouse monoclonal anti-GAPDH	EMD Millipore	Cat# MAB374; RRID: AB_2107445
Mouse monoclonal anti-Tropomyosin	DHSB	Cat# CGbeta6; RRID: AB_10573118
Alexa Fluor 488 goat anti-mouse IgG H+L	Thermo	Cat# A-11001; RRID: AB_2534069
Alexa Fluor 546 goat anti-rabbit IgG1	Thermo	Cat# A-21123; RRID: AB_2535765
Peroxidase-IgG Fraction Monoclonal Mouse Anti-Rabbit IgG, Light Chain Specific	Jackson ImmunoResearch Labs	Cat# 211-032-171; RRID: AB_2339149
Peroxidase-AffiniPure Donkey Anti-Mouse IgG antibody	Jackson ImmunoResearch Labs	Cat# 715-035-150; RRID: AB_2340770
Chemicals, Peptides, and Recombinant Proteins		
DAPI	Thermo	Cat# D1306
VFELIQNGWFLSQVR (57-71; 918.4938 2+)	This paper	N/A
FSLGAITSNNSGIYR (81-95; 800.4099 2+)	This paper	N/A
WTMLSNAVEVTGK (114-126; 718.3661 2+)	This paper	N/A
QEGVDGVQKPDVQHK (166-180; 555.2848 3+)	This paper	N/A
NAAEFQLR (250-257; 474.7485 2+)	This paper	N/A
IHGFSPTR (265-272; 457.7458 2+)	This paper	N/A
DAILYYVNLK (273-282; 606.3372 2+)	This paper	N/A
ELDNPGPFTC [+57]R (283-293; 653.2982 2+)	This paper	N/A
DLEPGSTVQLR (332-342; 607.8224 2+)	This paper	N/A
VNGPPPKPR (414-422; 321.1908 3+)	This paper	N/A
STVHLGQEAIFR (429-440; 679.3648 2+)	This paper	N/A
STVHLGQEAIFR (429-440; 453.2456 3+)	This paper	N/A
VSMELVR (448-454; 417.2311 2+)	This paper	N/A
TPFAVASTR (459-467; 475.2587 2+)	This paper	N/A
Critical Commercial Assays		
RNeasy Plus Mini Kit	QIAGEN	Cat# 74136
TRIzol Reagent	Thermo	Cat# 15596018
RNAlater Solutions for RNA Stabilization and Storage	Thermo	Cat# AM7020
RNAqueous™-Micro Total RNA Isolation Kit	Thermo	Cat# AM1931
RQ1 RNase-Free DNase	Promega	Cat# M6101
BCA Protein Assay Kit	Thermo	Cat# 23225
Tissue-Tek OCT Compound	Sakura	Cat# 4583
Deposited Data		
MS/MS Raw files and MaxQuant analysis files	This paper	ProteomeXchange: PXD020139
RNA-seq Raw data for adult C57 hearts	This paper	GEO: GSE182691
RNA-seq Raw data for E9.5 C57 hearts	This paper	GEO: GSE182690

Continued

REAGENT or RESOURCE	SOURCE	IDENTIFIER
Experimental Models: Organisms/Strains		
Mouse: C57BL/6J	The Jackson Lab	Stock No: 000664
Mouse: PWK/PhJ	The Jackson Lab	Stock No: 003715
Mouse: A/J	The Jackson Lab	Stock No: 000646
Mouse: WSB/EiJ	The Jackson Lab	Stock No: 001145
Mouse: CAST/EiJ	The Jackson Lab	Stock No: 000928
Mouse: 129S1/SvlmJ	The Jackson Lab	Stock No: 002448
Mouse: NZO/H1LtJ	The Jackson Lab	Stock No: 002105
Mouse: NOD/ShiLtJ	The Jackson Lab	Stock No: 001976
Mouse: FCG model	Arthur Arnold's Lab	N/A
Mouse: XY* model	Arthur Arnold's Lab	N/A
Mouse: A1bg^{flox}	Frank Conlon's Lab	UNC_AMC1005
Mouse: Tg(Tnnt2-cre)5Blh/JiaoJ	The Jackson Lab	Stock No: 024240
Oligonucleotides		
Primer for genotyping the *Sry* gene, Fwd: 5'-TTGTCTAGAGAGCATGGAGGGCCATGTCAA-3'	This paper	N/A
Primer for genotyping the *Sry* gene, Rev: 5'-CCACTCCTCTGTGACACTTTAGCCCTCCGA-3'	This paper	N/A
Primer for genotyping the control gene (*Fabpi*), Fwd: 5'- CCTCCGGAG AGCAGCGATTAAAAGTGTCAG-3'	This paper	N/A
Primer for genotyping the control gene (*Fabpi*), Rev: 5'- TAGAGCTTTGCC ACATCACAGGTCATTCAG-3'	This paper	N/A
Primer for genotyping the Tnnt2-cre, Fwd: 5'-TTGTTCCTTTAGCCCTGTGC-3'	The Jackson Lab	39788
Primer for genotyping the Tnnt2-cre, Rec: 5'-AGGCAAATTTTGGTGTACGG-3'	The Jackson Lab	oIMR9074
Primer for genotyping the A1bg flox, Fwd: 5'- GTGTTCTTGGGAAGGGTTCA-3'	This paper	A1bg 3ScF1
Primer for genotyping the A1bg flox, Rev: 5'-CAGCCAGAACCCTTAGTGTAGT-3'	This paper	A1bg 3ScR1
Software and Algorithms		
ImageJ (version 1.53a)	National Institutes of Health	https://imagej.net/Downloads
R v3.7	R Project for Statistical Computing	https://www.r-project.org/
Proteome Discoverer 2.3	Thermo Scientific	N/A

RESOURCE AVAILABILITY

Lead contact
Further information and requests for resources should be directed to and will be fulfilled by the Lead Contact, Frank L. Conlon (frank_conlon@med.unc.edu).

Materials availability
The new mouse line (*A1bg flox*) is available upon request from the Lead Contact.

Data and code availability
The RNA-seq raw data have been deposited at the GEO repository and are publicly available as of the date of publication, and the accession numbers are listed in the key resources table. The MS Proteomics data, including the MS raw files, have been deposited at the ProteomeXchange Consortium repository and the identifier is listed in the key resources table.

This paper does not report original code.

Any additional information required to reanalyze the data reported in this paper is available from the Lead Contact upon request.

EXPERIMETAL MODEL AND SUBJECT DETAILS

Mouse

The founders of the Collaborative Cross (CC) and the strain of *Tnnt2$^{cre/+}$* mouse were obtained from the Jackson Lab, and housed at the Division of Laboratory Animal Medicine, University of North Carolina at Chapel Hill (UNC-CH). The FCG and XY* model mice were maintained by Arthur Arnold's lab at University of California, Los Angeles. The strain of A1bg flox mouse was generated at the Animal Model Core of UNC-CH. Mice were sacrificed at 8 weeks, and hearts were perfused with 1×PBS and dissected, snap frozen for proteomics or western blot analysis, or perfused with 4% paraformaldehyde (PFA)/0.1% Tween-20/PBS for immunohistochemistry staining or dissected and immediately homogenized in Trizol for RNA extraction for RNA-seq analysis. The C57 mice were used for timed mating, with the morning of detection of vaginal plug defining as E0.5. Both male and female mice were used. Mice were housed in plastic cages at controlled temperatures of 25 ± 1°C, on a 12-h light/12-h dark cycle, with lights on from 07:00–19:00. Standard rodent chow and water were provided throughout the study period. Research was approved by the Institutional Animal Care and Use Committee at UNC-CH and conformed to the Guide for the Care and Use of Laboratory Animals.

METHOD DETAILS

RNA-sequencing analysis

RNA extraction from individual adult heart (n=4 per sex) or E9.5 embryonic heart (4 biological replicates per sex, 6 hearts were pooled as one biological replicate) was performed as previously described (Wilczewski et al., 2018), Poly-A selected RNA-seq libraries preparation and sequencing reactions were conducted at GENEWIZ, LLC. (South Plainfield, NJ, USA). Samples were run on a HiSeq2500 (Illumina) with 2×150 bp paired end reads.

Sequence reads were trimmed to remove possible adapter sequences and nucleotides with poor quality using Trimmomatic v.0.36. The trimmed reads were mapped to the Mus musculus GRCm38 reference genome available on ENSEMBL using the STAR aligner v.2.5.2b. Unique gene hit counts were calculated by using featureCounts from the Subread package v.1.5.2. The hit counts were summarized and reported using the gene_ID feature in the annotation file. Only unique reads that fell within exon regions were counted. After extraction of gene hit counts, the gene hit counts table was used for downstream differential expression analysis. Using DESeq2, a comparison of gene expression between the customer-defined groups of samples was performed. The Wald test was used to generate p-values and log$_2$(fold changes). Genes with an adjusted p-value < 0.05 and absolute log$_2$(fold changes) > 0.5 were called as differentially expressed genes for each comparison.

Dissection and sex genotyping of E9.5 embryonic hearts

Each E9.5 heart was dissected in ice-cold PBS and snap frozen in liquid nitrogen individually for proteomics analyses or individually stored in RNAlater Solutions in -20°C until use, primers for genotyping the sex of each embryonic heart were listed in the key resources table.

Immunohistochemistry

Hearts from two male and two female C57BL/6J mice were fixed in 4% PFA/0.1% Tween-20/PBS at 4°C overnight, dehydrated by sucrose gradient and embedded in OCT followed by cryostat sectioning. Immunofluorescent staining was performed with antigen retrieval on 8 μm coronal cryosections as previously described (Dorr et al., 2015). Primary and secondary antibodies information were listed in the key resources table. Immunohistochemistry images were captured on a Zeiss LSM 700 laser scanning confocal microscope. ImageJ (NIH) was used for image analysis and standard image processing.

Western blot

Snap frozen hearts (3 males and 3 females) were homogenized using a mortar and pestle in liquid nitrogen. Lysed the heart homogenate on ice for 30 min in RIPA buffer (50 mM Tris8.0, 0.5% Sodium Deoxycholate, 150 mM NaCl, 1% Triton-X 100, 0.1% SDS) with protease inhibitors. Quantification of protein concentration in total lysates was performed by using BCA Protein Assay Kit (Thermo #23225). Equal protein amount (40 μg) from each sample was loaded for SDS-PAGE gel electrophoresis. Western blots were blocked with 5% milk/TBST at room temperature for 1 hr, and then probed with specific primary antibodies overnight at 4°C and followed by probing with secondary antibodies at room temperature for 1 hr. Antibody-antigen complexes were visualized using an ECL Western Blotting Analysis System (Amersham). Primary and secondary antibodies information were listed in the key resources table. Quantifications of protein bands from western blot films was performed with ImageJ, relative expression of each target protein were determined by the ratio to GAPDH. Significance between male and female in protein expression was determined by Student's t-test based on bands intensity quantification.

Generation of cardiac A1bg knockout mouse

Cas9 guide RNAs targeting the mouse *A1bg* 3rd intron (protospacer sequence 5'- GGCCCCTAGAGGCTTGTAAG -3') and downstream of the *A1bg* 7th exon (protospacer sequence 5'- GGGATATGGTGTCTGTAAAG -3') were cloned into a T7 promoter vector followed by T7 in vitro transcription and spin column purification, with elution in microinjection buffer (5 mM Tris-HCl pH 7.5, 0.1 mM EDTA). The donor plasmid included a 3.1 kb critical region encompassing exons 4 through 7 of the mouse A1bg gene flanked

by loxP sites and homology arms (Figure 6I). The donor vector was prepared by Qiagen High Speed Maxiprep protocol and resuspended in microinjection buffer. Recombinant Cas9 protein was expressed in E. coli and purified by the UNC Protein Expression and Purification Core Facility. C57BL/6J zygotes were microinjected with 400 nM Cas9 protein, 25 ng/μL each guide RNA and 20 ng/μL donor plasmid in microinjection buffer. Injected embryos were implanted in recipient pseudopregnant females. Resulting pups were screened by PCR for the presence of the loxP insertion events. A male founder was identified with homologous integration of the donor vector. The founder was mated to wild-type C57BL/6J females to establish a colony with the flox allele.

Founding $A1bg^{flox/+}$ males were bred to wildtype mice for 2 generations, and the genotypes of $A1bg^{flox/+}$ founding males and all F2 offspring were confirmed by sequencing and PCR (Figure S6G). To generate a cardiac conditional allele, $A1bg^{flox/+}$ mice were crossed with the cardiomyocyte specific $Tnnt2^{cre/+}$ (Jiao et al., 2003) to generate $Tnnt2^{cre/+};A1bg^{flox/+}$, these mice were then intercrossed to generate the homozygosity $A1bg$-KO ($Tnnt2^{cre/+};A1bg^{flox/flox}$) mice.

Echocardiography
Cardiac function of conscious 12 week-old KO ($Tnnt2^{cre/+};A1bg^{flox/flox}$) and $control$ ($A1bg^{flox/flox}$) mice (both male and female mice for each genotype were used, and 3-4 mice per genotype per sex) were assessed by thoracic echocardiography using the Vevo 2100 High-Resolution Micro-Imaging System with MS-330D ultrasound transducer (Visual Sonics, Inc.) as previously described (Kennedy et al., 2017). Briefly, mice were anesthetized with 5% Isoflurane and were placed on a warmed platform in the supine position for imaging, with 0.25-0.5% Isoflurane maintenance. A topical hair removal agent was used on the chest and abdomen of mice, a 40 MHz pediatric probe was used to capture 2-dimensional guided M-mode views of the long and short axes at the level of papillary muscle. Visual Sonics Analytic software was used to determine mean ventricular wall and interventricular septum thickness, as well as the left ventricle diameter from at least 5 consecutive cardiac cycles. All imaging was done by trained technicians blinded to the genotypes of the animals.

Mass spectrometry sample preparation
A total of 32 founder strain hearts (8 founder strains, 2 male and 2 female replicates for each strain), 12 FCG hearts (4 FCG genotypes, 3 replicates for each genotype), and E9.5 hearts (3 male and 3 female replicates, 20 pooled hearts for each) were prepared for mass spectrometry analysis with either TMT 10-plex labeling (founder strain hearts and FCG hearts) or with label-free quantitation (E9.5).

Subcellular fractionation was performed on the founders hearts with 2 biological replicates per strain. Briefly, hearts were diced, snap frozen in liquid nitrogen, and then blended in a stainless-steel waring blender. Tissue powder was dissolved in a modified NIB-250 buffer, containing 10 mM Tris, pH 7.4, 250 mM sucrose, 1mM EDTA, 0.15% NP-40, 10 mM sodium butyrate, 1 mM PMSF, and 1X HALT protease and phosphatase inhibitor (Pierce). After gentle centrifugation at 400 rpm, the supernatant (cytosolic fraction) was transferred to a new low-bind tube and the pellet (nuclear fraction) was resuspended in lysis buffer (20 mM K-HEPES, pH 7.4, 110 mM KOAc, 2 mM MgCl2, 0.1% Tween-20, 1 mM ZnCl2, 1 mM CaCl2, 150 mM NaCl, 0.5% Triton x100, 1X HALT protease and phosphatase inhibitors). Following subcellular fractionation, lysates were reduced and alkylated with 25 mM tris(2-carboxyethyl) phosphine (TCEP, Pierce, Waltham, MA) and alkylated with 50 mM chloroacetamide (CAM, ThermoFisher Scientific, Waltham, MA) for 20 min at 70°C, methanol/chloroform precipitated, dried briefly in speed vac, and resuspended in 25 mM HEPES, pH 8.2. BCA assay was performed to estimate protein concentration, and 50 μg of protein was digested with sequencing grade trypsin (Promega) at 1:50 trypsin:sample protein amount for 14 hrs on a ThermoMixer at 37°C and 600 rpm. Samples were concentrated in a vacuum centrifuge to generate 50 mM HEPES, pH 8.2, adjusted to 20% ACN, and labeled with 10 μL of 15.4 μg/μL of the corresponding TMT 10-plex reagent for 1 hr at room temperature with shaking at 1000 rpm. The labeling reaction was quenched with 7 μL of 5% hydroxylamine, and the equal amount (2 μL) of labeled peptides were then mixed with 0.1% trifluoroacetic acid (TFA) (Pierce) to generate a test mix which was desalted by StageTip fractionation with Empore C18 filters (3M) (Rappsilber et al., 2007). Disks were first charged with a 100% acetonitrile (ACN) wash, followed by 2 conditioning washes with 0.1% TFA. Test mix samples were then applied to the StageTip, washed twice with 5% ACN with 0.1% TFA, and eluted with 70% ACN with 1% FA. Eluted samples were then dried in a vacuum centrifuge, resuspended in 5 μL of 2% ACN with 1% FA. Once the test mix was analyzed by mass spectrometry (described below), equal amounts of each TMT channel were mixed according to the derived ratios generated from the Proteome Discoverer 2.2 search of the data (described below).

The sex reversed FCG mouse hearts (3 biological replicates per genotype) were prepared in a similar manner as the founders samples, however, subcellular fractionation was not performed on these hearts. Isolated hearts were first minced into thin slivers and homogenized in 4 mL of 50 mM Tris-HCl, pH 8.0, 100 mM NaCl, 0.5 mM EDTA, and 1x HALT protease and phosphatase inhibitor cocktail (Pierce) with 40 strokes in a Tenbroeck homogenizer. Lysates were then transferred to 15 mL tubes and mixed 1:1 with the same buffer containing 4x SDS to generate a final SDS concentration of 2% SDS. These samples were then heated at 95°C for 5 min and then sonicated in a cup horn sonicator (1 sec pulses, medium power) individually for 20 seconds, repeated 3 times or until no insoluble material remained. Protein concentration was estimated using the BCA assay, 50 μg of protein for each sample was aliquoted and reduced and alkylated, methanol/chloroform precipitated, resuspended with 25 mM HEPES, pH 8.2, and digested with trypsin, as with the Founder line hearts above. TMT labeling and test mix desalting were performed as described earlier. The TMT mixes for the founders and FCG mice were subsequently desalted and fractionated with a Pierce High pH Reversed-Phase Peptide Fractionation Kit (Thermo #84868), as per the manufacturer's protocol.

The Klinefelter series hearts (4 biological replicates of each of the 4 genotypes) were prepared in the exact same manner as the FCG mouse hearts. Two TMT 10-plex kits were used for this analysis, with 2 replicates of each of the 4 genotypes randomly assigned

to each channel, and two reference channels were generated after digestion, one reference channel of an equal mixture of the 8 samples used within the plex, and a second reference channel made of all samples analyzed in this dataset.

Embryonic day 9.5 mouse hearts were prepared for label free quantitation. Due to the low amount of protein extracted per embryonic heart (∼4-6 μg per heart), 20 mouse hearts were combined per replicate, with three biological replicates performed per sex. Embryonic hearts were lysed in 50 mM Tris-HCl, pH 8.0, 100 mM NaCl, 0.5 mM EDTA, and 5% SDS with sonication in a cup horn sonicator (1 sec pulses, medium power) individually for 20 seconds, followed by heating at 95°C for 5 min, repeated 3 times or until no insoluble material remained. Samples were then reduced and alkylated with 20 mM TCEP and 40 mM CAM for 20 min at 70°C. The SDS lysate was then acidified with phosphoric acid to generate a final concentration of 1.2% phosphoric acid. Samples were then digested with an S-Trap (ProtiFi) following the manufacturer's protocol. Briefly, samples were adjusted to 90% methanol, applied to the S-Trap column, washed with S-Trap binding buffer (100 mM triethanolamine bicarbonate, pH 7.1, with 90% methanol), followed by the addition of 1 μg of trypsin in S-Trap digestion buffer (25 mM TEAB, pH 8), with digestion at 47°C for 1 hr. Digested peptides were sequentially eluted from the S-Trap column with 40 μL of 25 mM TEAB, pH 8.0, 0.2% FA, then 50% ACN with 0.2% FA. These elution steps were combined, dried in a vacuum centrifuge, and then dried peptides were fractionated with Pierce High pH Reversed-Phase Peptide Fractionation Kit, as with the FCG samples.

Peptide fractionation

Each TMT mix for the founders was fractionated by StageTip fractionation with Empore C18 filters (3M) as previously described (Federspiel et al., 2019). Briefly, samples were dried in a vacuum centrifuge and resuspended in 1% TFA. 5 C18 filter disks were packed into a pipette tip, and were first charged with 100% ACN, equilibrated with 1% TFA, and then samples were applied to the disks. For test mix TMT runs, samples were desalted with 0.5% FA with 5% ACN in UHPLC water and eluted with 0.5% FA with 70% ACN in UHPLC water. For quantitative TMT samples, appropriate amounts of each TMT channel were mixed according to the derived quantitative values, and these mixtures were dried in a vacuum centrifuge, resuspended in 1% TFA, and then desalted and fractionated by StageTip fractionation. Disks were first charged with 100%, equilibrated with 1% TFA, samples were loaded onto disks, desalted with 5% ACN in UHPLC water, and samples were eluted in 20 fractions with sequential elution (20 μL each) ranging from 0.04 M Ammonium Hydroxide/8% ACN to 0.04 M Ammonium Hydroxide/46% ACN. The twenty collected fractions were concatenated to 10 fractions by combining fraction 1 and 11, 2 and 12, etc. For the FCG and E9.5 hearts, desalting and fractionation was performed with Pierce High pH Reversed-Phase Peptide Fractionation Kits (Thermo Scientific) to generate 8 fractions per sample, as per the manufacturer's protocol. All fractions were dried to near dryness in a vacuum centrifuge and resuspended in 1% FA with 2% ACN in UHPLC water for liquid chromatography tandem mass spectrometry (LC-MS/MS) analysis.

Parallel reaction monitoring (PRM) sample preparation

Cardiac samples were prepared as described previously, protein concentration was estimated by a BCA assay, and 50 μg of protein (ranging from 20 μL to 120 μL) was aliquoted and adjusted to 5% SDS and prepared for digestion with an S-Trap (Protifi, C02-micro-80) following the manufacturer's protocol. Samples were first reduced and alkylated with a final concentration of 20 mM TCEP and 40 mM CAM for 20 minutes at 70°C, and subsequently acidified with 1.2% phosphoric acid. To each sample, a sufficient amount of 90% methanol in 100 mM triethanolamine bicarbonate (TEAB, pH 7.1, ThermoFisher Scientific, 90114, pH adjusted from pH 8 to pH 7.1 with phosphoric acid) was added to achieve 80% methanol and 90 mM TEAB (ranging from 165 μL to 1 mL). Samples were then loaded onto the S-trap column by multiple sequential additions of 185 μL of the samples (in instances where the volume was greater than 185 μL due to low protein concentration in some samples) by centrifugation until the solution completely passed through the S-Trap column. Once samples were loaded onto the S-Trap column, samples were washed seven times with 150 μL of 90% methanol and 100 mM TEAB (pH 7.1), five times with 150 μL of 80% methanol and 20% chloroform, and then a final five times with 150 μL of 90% methanol and 100 mM TEAB (pH 7.1). Samples were then digested with 1 μg of sequencing grade trypsin (ThermoFisher Scientific, PI90059) in 100 μL 25 mM TEAB (pH 8.0) overnight at 37°C without shaking in a ThermoMixer (Eppendorf). Peptides were eluted with three sequential washes of 40 μL of 25 mM TEAB (pH 8.0), 40 μL of 0.2% FA, and 70 μL of 50% ACN with 0.2% FA by centrifugation. These elutions were pooled, dried down in a speed-vac, resuspended in 100 μL 0.1% TFA to precipitate insoluble material and centrifugated at max speed, dried down again, and then resuspended in 100 μL of 1% FA in 1% ACN to achieve a protein concentration of 0.5 μg/ μL, and 2 μL of each sample was analyzed on a Q-Exactive HF mass spectrometer.

PRM LC-MS/MS analysis

Samples for PRM analysis were analyzed on a Q-Exactive HF mass spectrometer equipped with a Nanospray Flex Ion Source (ThermoFisher Scientific). Peptides were analyzed for nLC-MS analysis with a Dionex Ultimate 3000 nRSLC (ThermoFisher Scientific) equipped with a 50 cm fused silica capillary (75 μm x363 μm) column packed in-house with ReproSil-Pur C18 packing material (ReproSil-Pur 120 C18-AQ 1.9 μm, ESI Source Solutions r119.aq.0001). Peptides were resolved with a 71-minute gradient at a flow rate of 250 nL/min using Solvent A (99.9% LC-MS grade water with 0.1% formic acid) and Solvent B (99.7% LC-MS grade acetonitrile, 0.2% LC-MS grade water, 0.1% formic acid; 5 to 35% B over 60 minutes, 35 to 97% B over 1 minute, and held at 97% for 10 minutes). One full duty cycle of the instrument consisted of a single Full-MS1 scan followed by 4 PRM scans. For the Full-MS1 scan, the instrument was set to a 350-1,800 m/z full scan range with a 15,000 resolution, 15 ms MIT, and 1e6 AGC target. For the PRM scans, the instrument was set to a 30,000 resolution, 25 ms MIT, 5e5 AGC target, 1.2 m/z isolation window, NCE of 27, and a fixed first mass of 125 m/z. Spectrum data for both the Full-MS1 and PRM scans were recorded in profile.

QUANTIFICATION AND STATISTICAL ANALYSIS

Mass spectrometry analyses

TMT labeled tryptic peptides (founder line strains and FCG strains) were separated with an EasyNano nLC1000 UHPLC (ThermoFisher Scientific) (running mobile phases: A (aqueous), 0.1% FA/H20; B (organic), 0.1% FA/97% ACN/2.9% H20) coupled online to an EASY-Spray ion source and a Q Exactive HF (ThermoFisher Scientific). Samples were separated on a nanocapillary reverse-phase Pep-MapC18 analytical column (75 μm by 500 mm; particle size 1.8 μm) (Thermo Scientific,) heated to 50°C with a 120-min linear gradient (6%-29% mobile phase B) at a flow rate of 250 nL/min. MS1 spectra were acquired over the m/z range from 400-1800 at a resolution of 120,000, an AGC of 3×10^6, and a Maximum Injection Time (MIT) of 30 ms. Data-dependent selection and fragmentation was performed on the top twenty most intense precursor ions by collision-induced dissociation and MS2 scans were acquired at a resolution of 45,000 with an AGC setting of 1×10^5, a MIT of 72 ms, and an isolation window of 0.8 m/z. Label-free analysis (E9.5 heart fractions) was performed in the same manner, except samples were separated with a 150-min gradient (5%-30% mobile phase B), and data-dependent acquisition was performed at a resolution of 15,000, with an AGC of 1×10^5, and a MIT of 150 ms.

Database searching and reporter ion quantitation or label-free quantitation

For the founder and FCG strains, Proteome Discoverer 2.2.0.388 was used to search the LC-MS/MS data utilizing a fully tryptic By-onic search node in the processing workflow, searching against a combined Uniprot database containing M. musculus canonical protein sequences with common contaminants (17537 entries, downloaded 2018_08). A max of 2 missed cleavages were allowed, and peptides were required to have 5 ppm precursor accuracy and 10 ppm fragment accuracy. Peptide modifications included static cysteine carbamidomethylation, dynamic methionine oxidation, dynamic N-terminal methionine loss with N-terminal acetylation, dynamic asparagine deamidation, dynamic phosphorylation of serine, threonine, and tyrosine residues, and static TMT 10-plex labeling reagent on free peptide N-termini and on the ε-nitrogen on lysine residues. The reporter ion quantifier node was utilized for TMT fragment ion quantitation. In the FCG samples, we observed a distinct batch effect by PCA, we observed a distinct batch effect by PCA, where one of the four litters occupied a distinct PCA space from the others. Thus, data acquired from channels 126, 128C, 129N, and 129C in the TMT plex were excluded.

For the E9.5 hearts, Proteome Discoverer 2.4.305 was used to search the LC-MS/MS data utilizing a fully tryptic SequestHT search node in the processing workflow, searching against a combined Uniprot database containing M. musculus canonical protein sequences with common contaminants (17537 entries, downloaded 2018_08). A max of 2 missed cleavages were allowed and peptides were required to have 5 ppm precursor accuracy and 0.02 Da fragment ion accuracy. Peptide modifications included static cysteine carbamidomethylation, dynamic methionine oxidation, dynamic N-terminal methionine loss with N-terminal acetylation, dynamic asparagine deamidation, and dynamic phosphorylation of serine, threonine, and tyrosine residues. Statistical analysis of male/female differential abundance was performed using the Background test in Proteome Discoverer.

Gene set enrichment analyses

Enrichment analyses were adapted from FIRE/iPAGE method (Goodarzi et al., 2009). The ratios of protein (RNA) abundance between males and females (M/F), or $\log_e$(protein abundance) derived from Bayesian analysis, were sorted from higher to lower. Sorted ratios were divided into n = 9 bins, which contain the same number of proteins (transcripts). C5 GO gene sets curated by MSigDB was used to annotate proteins (http://software.broadinstitute.org/gsea/msigdb/collections.jsp).

For each GO gene set, an array C of $2\times N$ was created, where N represents the number of bins. C(0,j) indicates the number of genes in the jth ($i\leq j\leq N$) bin but not included in the GO term being analyzed; C(1,j) represents the number of genes in the jth bin and included in the GO term. The mutual information (MI) of each bin in C was calculated using scikit-learn mutual_enrichment_score function, as

$$MI = \sum_{i=0}^{1}\sum_{j=1}^{N}P(i,j)log\frac{P(i,j)}{P(i)P(j)}, \text{ where } P(i,j)=\frac{C(i,j)}{N}, P(i)=\sum_{j=1}^{N}P(i,j), \text{ and } P(j)=\sum_{i=0}^{1}P(i,j).$$ The MI scores represents the enrichment levels of the term being analyzed in each bin. To calculate z-scores for MI scores, we created a null distribution of the MI scores with 1,000 permutations with the same number of terms. Z-scores were defined as $\frac{MI-\mu}{\sigma}$, where μ and σ represent the mean and standard deviation, respectively.

To determine the level of enrichment, we defined the enrichment scores (ESj) of the jth bin as $s \times log_{10}p$ − value of the hypergeometric distribution, where s represents 1 or -1 as described below. The p-value for the enrichment score was calculated by the hypergeom function of Scipy as $min(p_{over},p_{under})$, where $p_{over}(X\geq x)=\sum_{k=x}^{N}\frac{\binom{m}{k}\binom{M-m}{n-k}}{\binom{M}{n}}$, and $p_{under}(X\leq x)=\sum_{k=0}^{x}\frac{\binom{m}{k}\binom{M-m}{n-k}}{\binom{M}{n}}$. M,

C, k and x represent $C=\sum_{i=0}^{1}\sum_{j=1}^{N}C(i,j), C(j)=\sum_{i=0}^{1}C(i,j), C(1)=\sum_{j=1}^{N}C(1,j)$, and $C(1,j)$, respectively. If $p_{over}>p_{under}$, s represents 1, otherwise -1. To estimate the degree of enrichment for male or female, we calculated the enrichment bias scores (ES_{bias}), defined as $ES_{bias}=\sum_{j=1}^{[N/2]}C(1,j)ESj-\sum_{[(N+3)/2]}^{N}C(1,j)ESj$. ES_{bias} were sorted from the highest to the lowest, and the top 200 terms were selected

for z-score calculation and heatmap plotting. Heatmaps of the ES values were plotted with matplotlib and seaborn packages in Python.

Bayesian inference analysis

Bayesian inference analyses were conducted using RStan in R (ver. 3.6.2). For the founders samples, we aim to obtain the posterior distributions of protein abundances contributed by sex and strain. We denoted the quantified protein abundance, average reference abundance, batch effect, sex effect, and strain effect as μ_{data}, $\mu_{reference}$, μ_{batch}, μ_{sex}, and , respectively, and $\mu_{data} = \mu_{reference} + \mu_{batch} + \mu_{sex} + \mu_{strain}$. We used a normal distribution as a prior for batch effect, and uniform priors for reference average, sex effect, and strain effect. A flat uninformative prior was used for the standard deviation of data σ_{data} given no prior knowledge. A normal distribution was used to fit the posterior distribution: $\text{Norm}(\mu_{data}, \sigma_{data})$. No-U-Turn sampler (NUTS) was used for sampling, with 3 chains, 4000 iterations and 1000 warmup iterations. Proteins whose credible intervals are exclusively positive or negative are considered differential. For the FCG samples, sex and strain effects were replaced by chromosomal and gonadal effects, denoted as μ_{chrom} and μ_{gonad}, and $\mu_{data} = \mu_{reference} + \mu_{batch} + \mu_{chrom} + \mu_{gonad}$. The same MCMC settings were used for this analysis as described above. For the XX:XY*X and XY*:XXY* comparisons of Klinefelter series samples, the quantified protein abundance is modeled as $\mu\_data = \mu\_reference + \mu\_chrom$, and the analyses were conducted as described above.

PRM data analysis

RAW files containing targeted PRM LC-MS/MS spectra were imported into Skyline to extract product ion chromatograms (XICs) and to calculate peak areas. The PRM method monitored 4 mouse proteins: A1bg as a protein that exhibited distinct cardiac differences between male and female mice, and Tuba1b, Gapdh, and H2bc14 to confirm efficient nuclear or cytoplasmic fractionation. For A1bg, thirteen prototypic peptides were selected for PRM analysis based upon ion intensity, peak area reproducibility, and liquid chromatography reproducibility from unscheduled analysis of each of the strains analyzed. From this initial analysis, scheduled runs were performed, and the measured peptide peak areas were scaled to the total average MS1 intensity in each PRM injection, and normalized peptide peak areas were summed from peptides with coefficients of variation (CVs) less than 20% across biological replicates (Figure S6F) of mouse strains and genders. The resulting normalized peak areas were analyzed in GraphPad Prism. A minimum of two peptides per protein were selected for quantification, and statistical analyses were performed with Student's t-test.